UNIVERSITY OF CALIFORNIA SAN DIEGO

Designing selective catalysts for production of formic acid through electrochemical reduction of CO_2

A Thesis submitted in partial satisfaction of the requirements
for the degree Master of Science

in

Chemical Engineering

by

Vivek Shastry Devalla

Committee in Charge:

Professor David P. Fenning, Chair
Professor Zheng Chen
Professor Ping Liu

2023

The Thesis of Vivek Shastry Devalla is approved, and it is acceptable in quality and form for publication on microfilm and electronically.

University of California San Diego

2023

TABLE OF CONTENTS

LIST OF FIGURES

LIST OF TABLES

ACKNOWLEDGEMENTS

First and foremost, I would like to express my gratitude to my advisor, Professor David P. Fenning, for his unwavering support throughout my M.S. journey. His patience, trust, motivation, enthusiasm, and extensive knowledge have been instrumental in making this dissertation possible. I would also like to extend my gratitude to our collaborator, Prof. Andrea R. Tao and Alex Fuqua for their immense role and knowledge in synthesizing and characterizing copper sulfide nanomaterials. I am also deeply thankful to the other members of my thesis committee, Prof. Zheng Chen, and Prof. Ping Liu, not only for their valuable comments on my thesis but also to widen my knowledge and inquisitiveness from the courses I have taken from them.

I also want to extend my thanks to Dr. Taewoo Kim, who has been an exceptional mentor, assisting me with daily lab matters, troubleshooting the parameters in electrolyzer, and instilling in me a meticulous "attention to detail" perspective. I would like to extend my sincere appreciation to all my colleagues in the Fenning lab and at UC San Diego. Your exceptional talent and willingness to support me have been invaluable whenever I felt lost.

Lastly, but certainly not least, I extend my sincere appreciation to my parents and sister for their unwavering support, and motivation, despite being 10,000 miles apart. I deeply value everything you have done for me, and I pledge to always make you proud. I am grateful for the unwavering support of my friends and family, both in India and San Diego.

Chapter 2, in full, is currently being prepared for submission for publication of the material "Modulating proton availability on the Copper sulfide surface to improve the selectivity of CO2 electroreduction to Formate", **Vivek S. Devalla**, Alexander Fuqua, Andrea R. Tao and David P. Fenning. The dissertation author was one of the primary investigators and author of this material.

Chapter 3, in full, is currently under review for the publication of the material "Tuning oxidation state of SnO_x and Mass Transport to Enhance Catholyte-Free CO_2-to-Formate Electrolysis", Taewoo Kim, **Vivek S. Devalla**, Sean P. Dunfield, Sara Dorr, Moses Kudor, Apoorva Gupta, Jack Palmer and David P. Fenning. The dissertation author was one of the investigators and second author of this material.

ABSTRACT OF THE THESIS

Designing selective catalysts for production of formic acid through electrochemical reduction of CO_2

by

Vivek Shastry Devalla

Master of Science in Chemical Engineering

University of California San Diego, 2023

Professor David P. Fenning, Chair

Transforming carbon dioxide (CO_2) into valuable chemical feedstocks through electrochemical processes powered by renewable electricity shows promise in achieving carbon neutrality. However, the development of effective and selective catalysts is essential for enabling energy-efficient conversion. The activity and selectivity of the reaction towards formic acid production are governed by the stabilization of the *OCHO intermediate on the catalyst surface.

This thesis presents strategies for designing active electrocatalysts that exhibit improved selectivity towards formic acid in CO_2 electrolysis by manipulating the chemical environment surrounding the catalyst. Introducing a partial positively charged copper species on the surface in the form of copper sulfide stabilizes the *OCHO intermediate on the catalyst surface. The ligand plays a key role in supplying the proton required for the reduction of CO_2 to formate, and that an optimum pKa value ligand is beneficial for improved selectivity towards formate. Another aspect involves tuning the chemical state of tin oxide catalyst surfaces. By favoring a Sn (II) rich initial surface oxidation state, the selectivity and energy efficiency of formate generation are improved, offering a potential near-term solution for carbon-negative CO_2 electrolysis. Optimal design of electrolyzers is also crucial for facilitating the mass transport of CO_2, thereby increasing industrial relevance. These discoveries underscore the importance of chemical environment surrounding the catalyst, and chemical state in the efficient design of CO_2 reduction catalysts to formic acid and providing fundamental guidelines and direction towards achieving carbon-neutral CO_2 conversion.

Chapter 1

Introduction

1.1 Electrochemical CO_2 Conversion: A path to green chemicals

Figure 1.1 shows the pie chart of sources of greenhouse gas emissions in the US in 2021[1]. Among these greenhouse gases, CO_2 contributes 79.4% which is equivalent to 9 gigatons of CO_2 emissions in the atmosphere due to anthropogenic sources [2]. If we focus on each of these sectors, a huge global dependence on fossil-based fuels and chemicals to thrive the present global economy is evident. Fossil fuels being a great resource of energy has its downsides, one of them being the rising CO_2 levels.

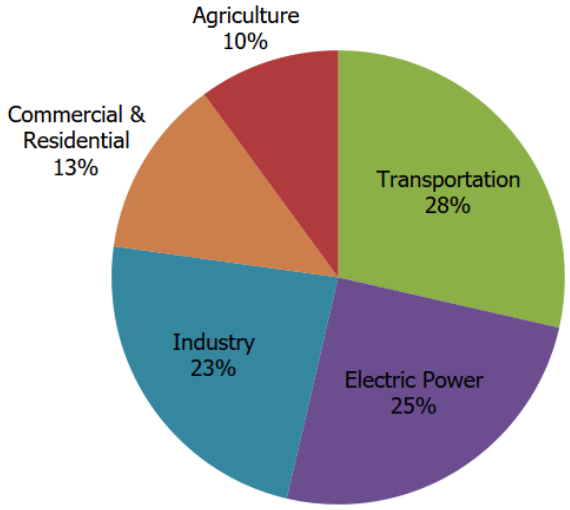

Figure 1.1. Emissions of greenhouse gases by sector in the U.S

This rising CO_2 levels in the atmosphere has caught the global attention due to its crucial role in destabilizing the natural cycle and thereby leading to climate change. To combat climate change and its impacts, an international treaty was adopted in 2015, also known as the Paris agreement.[3] This led to setting up of various frameworks to limit the global warming to 2℃ above pre-industrial levels, while also striving to pursue efforts to limit the temperature increase to 1.5℃ to protect earth's existing biomes.

Figure 1.2 shows the CO_2 concentration in the atmosphere over time from pre-industrial levels [2] and the correlation of CO_2 concentration with the temperature rise. It is evident from these figures that the global efforts to curb the CO_2 level is falling behind when compared to the present CO_2 levels and the CO_2 concentration for 1.5℃.

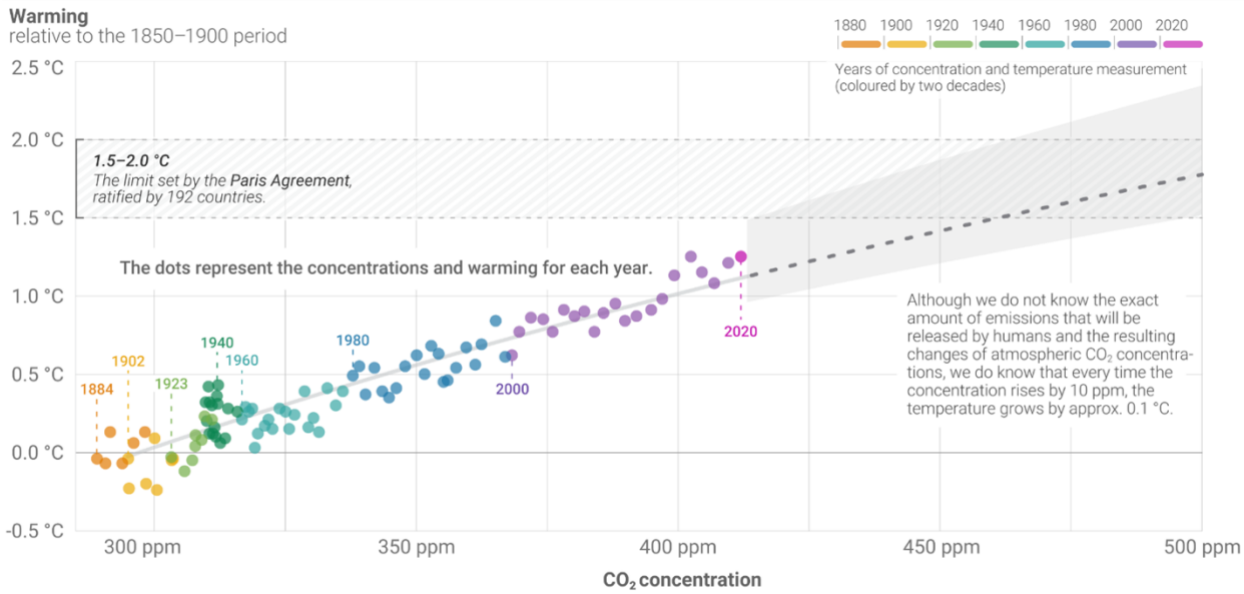

Figure 1.2. Correlation between temperature rise and concentration of CO_2 in the atmosphere where the dots indicate concentrations and warming for each year.

Scientists and researchers around the globe have been working on renewable energy sources, such as solar and wind energy trying to improve their efficiencies and bringing down the cost for utilizing renewable sources of energy. As we can see in the figure 1.3 [4], the cost of renewable electricity has drastically lowered in the past decade, thereby reducing the reliance on the fossil fuels for energy applications.

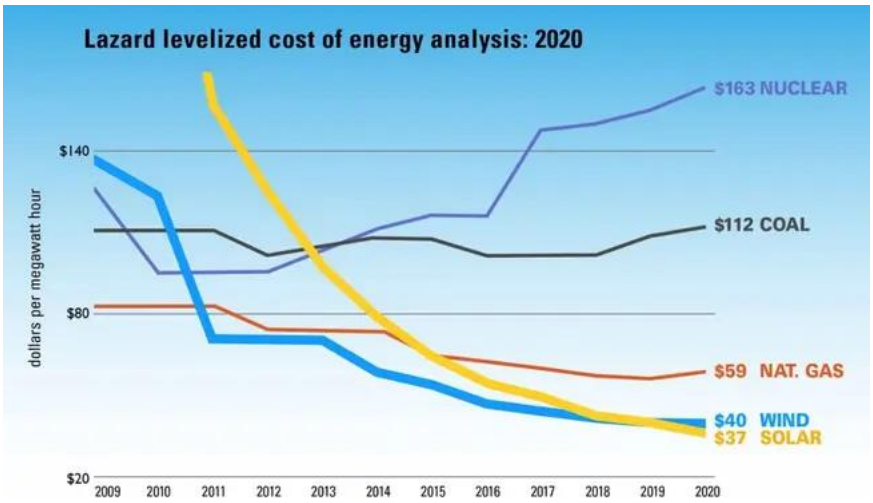

Figure 1.3. Lazard Levelized Cost of Energy (LCOE) Analysis 2020.

However, these renewable energy sources suffer from their intermittent nature, that is, the intensity of electricity being produced is fluctuating depending on the time of the day and month of the year, due to which the present grid system is affected.

Electrochemical conversion is a pathway to store this electrical energy in the form of chemical bonds. The electricity is used to break and make new bonds which can be stored as a chemical for long periods of time and can be converted back to electricity by reversing the chemistry. This is the concept behind the regenerative fuel cells and other electrocatalytic systems. Electrochemical conversion of CO_2 is a promising way to produce value from the waste. In aqueous systems, electrocatalytic CO_2 conversion can produce high value chemicals such as Ethylene and Ethanol, whose market sizes are $230 and $75 billions respectively. CO_2 electro-reduction can form other chemicals ranging from single carbon species such as carbon monoxide, formic acid to multi-carbon species such as 1 propanol. Off the shelf copper alone has shown to form 16 of these carbon-based chemicals.

According to the study done by De-Luna et al [5], the current production of carbon-based chemicals from fossil fuels is a major contributor to CO_2 emissions, highlighting the significant impact that synthesizing chemicals through electrochemical methods can have on achieving carbon neutrality, for example, producing ethylene and ethanol through CO_2 electro-reduction could lead to a reduction of 860 and 550 metric tons of CO_2 emissions, respectively. However, to synthesize these chemicals, significant amount of energy is drawn from the present electrical systems which questions the carbon neutrality standpoint since the electricity is derived majorly from fossil fuels. In this lieu, producing single carbon species such as formic acid is a beneficial route to address the carbon neutrality and carbon negative ecosystem. Figure 1.4 shows the plot between the net carbon neutral condition for a grid intensity and energy efficiency of the electrochemical system.

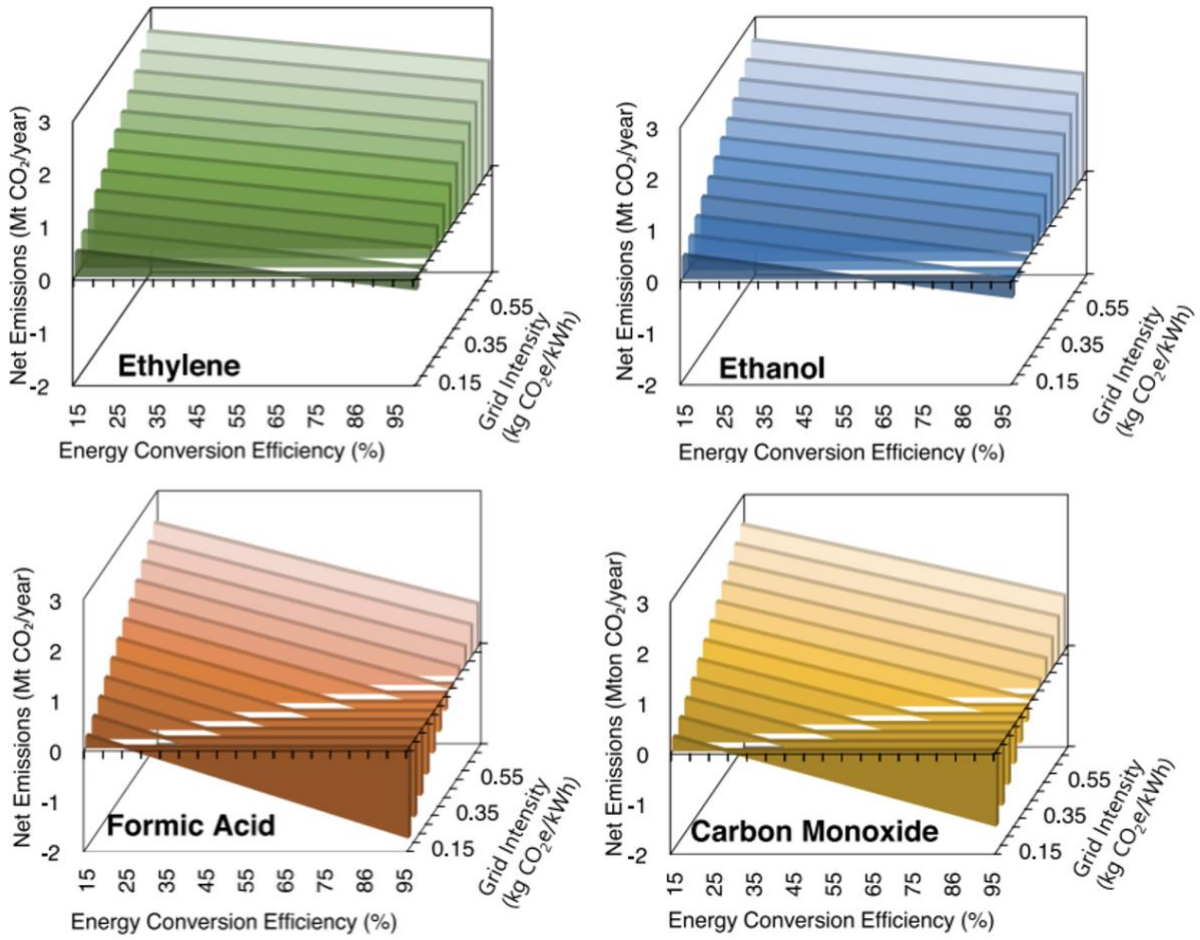

Figure 1.4. Carbon emissions assessment of formic acid, carbon monoxide, ethylene, and ethanol.

This implies that an electrochemical conversion of CO_2 to produce formic acid should be at lower applied cell voltages as well as the reaction needs to be highly selective towards formic acid to achieve a higher energy efficiency for production of formic acid. This calls for the need of better catalyst materials to steer the reaction towards formation of formic acid as well as doing these transformations at lower applied potential, which are discussed in this thesis.

1.2 Understanding the electrochemical CO_2 reduction reaction.

Before we dive into looking at the mechanism of CO_2 reduction reaction, it is important to study the theoretical limits posed by thermodynamics. We observe that the reduction potential for proton and CO_2 clubbed with proton are in proximity as summarized in Table 1.1. This implies that an electron which is energetic enough to drive CO_2 reduction chemistry is also energetic enough to drive proton reduction reaction to evolve hydrogen gas. This is the reason why we observe hydrogen gas as one of the products of CO_2 electrolysis, and thereby it is a parasitic reaction from CO_2RR point of view since it consumes the electrons which would have been driven to form carbon

products. Therefore, a catalyst needs to be designed in such a way that it would facilitate the desired product reaction pathway.

	E^0 (vs) RHE
$2H^+ + 2e^- \leftrightarrow H_2$	0.00 V
$CO_2 + 2H^+ + 2e^- \leftrightarrow CO + H_2O$	-0.10 V
$CO_2 + 2H^+ + 2e^- \leftrightarrow HCOOH$	-0.12 V
$CO_2 + 8H^+ + 8e^- \leftrightarrow CH_4 + 2H_2O$	+0.16 V
$2CO_2 + 12H^+ + 12e^- \leftrightarrow C_2H_4 + 4H_2O$	+0.08 V
$2CO_2 + 12H^+ + 12e^- \leftrightarrow C_2H_5OH + 3H_2O$	+0.09 V

Table 1.1. Thermodynamic understanding of CO_2 reduction reactions.

Figure 1.5 summarizes the mechanism of CO_2 reduction to a few carbon products such as methane, carbon monoxide, formic acid etc. As the number of electrons required for a reaction increases, the mechanism becomes complicated since there are multiple pathways through which the reaction coordinate can proceed towards a certain product.

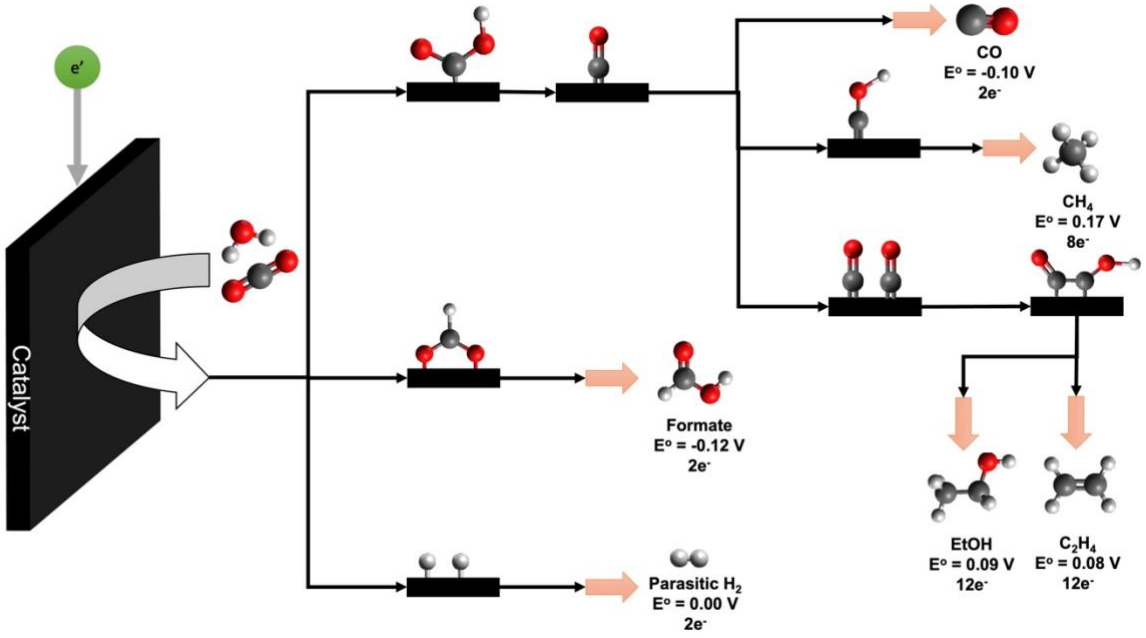

Figure 1.5. Mechanistic understanding of CO_2 reduction pathways.

To improve the efficiency of converting CO_2, it is crucial to have an optimal binding energy for the key intermediate in the reaction. Generally, it is believed that the initial intermediate in CO_2 reduction is either *COOH or *OCHO, as illustrated in figure 1.5. The choice between these two intermediates determines the entire reaction pathway, based on whether CO_2 is bound to the surface through a carbon atom or an oxygen atom.

When the initial intermediate is *OCHO, CO_2 reduction tends to produce formate, and it is widely accepted that *OCHO plays a significant role as a key intermediate for formate generation. Certain transition metals, such as Sn, Bi, In, and Pb, exhibit a preference for binding *OCHO rather than *COOH, resulting in a higher tendency for formate generation.

On the other hand, if CO_2 binds to the surface through a carbon atom, forming *COOH, the transition to *CO occurs rapidly. The binding energy of *CO plays a crucial role in determining the subsequent reaction paths, particularly to produce high-energy-density products. Weak binding of *CO to the catalyst surface leads to its easy release as the final product, CO, which is observed on surfaces like Ag and Au [6]. Conversely, if *CO binds extremely strongly, it hinders further reduction due to surface poisoning. Among other transition metals, Cu exhibits a moderate adsorption energy to *CO, allowing to produce value-added products such as hydrocarbons and oxygenates. However, its poor selectivity remains a significant challenge.

The ideal parameters to steer the reaction towards formic acid are, (i) optimum binding energy of the key reaction intermediate (*OCHO), (ii) surface electron density, (iii) proton availability. Some of these key attributes are discussed in the following chapters in this thesis.

1.3 Electrolyzer Configuration

1.3.1 Batch Cell (H-Cell):

For many years, extensive efforts have been focused on gaining a deep understanding of the reaction mechanisms and catalyst design parameters in conventional batch-type CO_2 conversion reactors operating in an aqueous phase. These reactors typically consist of a three-electrode system, comprising a working electrode (cathode), a reference electrode, and a counter electrode (anode). The electrolyte is divided into catholyte and anolyte compartments, separated by a membrane. A thin polymeric sheet with ion channels, allowing the passage of either cations or anions, is utilized as the membrane.

Throughout my masters, concerning the batch-type reactor, a Ag/AgCl(KCl gel) electrode (low profile, 3.5 mm OD, 74 mm length, Pine research) and a graphite rod (Pine research) are employed as the reference and counter electrodes, respectively. An anion exchange membrane (AEM, Selemion) is predominantly used due to preliminary tests in the lab indicating that a cation exchange membrane (CEM, Nafion) resulted in high ohmic resistance. A polished glassy carbon disk is serves as the substrate for the cathode, where catalytic materials are coated on the surface. CO_2 is continuously supplied into the electrolyte to ensure maximum availability of CO_2 at the catalytic sites.

Due to the low solubility of CO_2 in the aqueous electrolyte (approximately 34 mM), the CO_2 available to the catalytic sites is limited, presenting significant challenges in enhancing catalytic activity in terms of current density. Achieving high current density is crucial for industrial-level performance, where more than 500 mA cm-2 is required [5].

The design of each polycarbonate component (anolyte and catholyte chamber, cathode holder, glassy carbon disk holder, and end plates) is based on our lab's previous work [7] and modified through machining. Polycarbonate is chosen as the material due to its chemical compatibility with potassium bicarbonate and its pH range of 6 to 8, which is the electrolyte used in the system. CO_2 electrolysis is performed using a CO_2-saturated 0.7 M $KHCO_3$ solution as the electrolyte. The pH of the solution after a 30-minute CO_2 purging process is 7.6, which is used in the calculations to convert the scale from Ag/AgCl to RHE. It is necessary to purify the electrolyte before any CO_2 electrolysis to remove metallic impurities, which is discussed below. A dry CO_2 gas stream is introduced into the catholyte chamber through gas dispersion tubes with fine-sized pores (5x135 mm, porosity E filter, Aceglass) to facilitate mass transport. The CO_2 gas feed is also supplied to the anolyte chamber to achieve pH balance.

The electrolyte purification process consists of three steps, involving the regeneration of Chelex resin (product No. 1421253). To purify 250 ml of 0.7 M $KHCO_3$ solution, 9.38 g of Chelex resin is used. The Chelex resin is regenerated in a 1 M HCl solution for 12 hours under vigorous stirring, followed by washing and filtering with 5 L of deionized (D.I.) water using a 0.45-micron filter (Corning polystyrene). Subsequently,

the filtered resin is immersed in a 1 M KOH solution at 60°C for 24 hours under vigorous stirring, and then washed and filtered until the pH of the solution reaches neutral. During the 24-hour stirring process, a condenser (total reflux) is used to prevent changes in concentration due to solvent evaporation. The heated KOH solution should be cooled to room temperature during the neutralization process. Finally, the purified 0.7 M $KHCO_3$ solution is prepared by mixing the prepared 0.7 M $KHCO_3$ solution with the regenerated Chelex resin for 24 hours under vigorous stirring, followed by filtration.

It is important to ensure the purity of the components within the batch-type reactor for CO_2 electrolysis. Even trace amounts of metal components from previous electrolysis can have a detrimental effect on subsequent electrolysis. Therefore, it is recommended to clean the polycarbonate body with a diluted 10 vol.% HCl solution for at least an hour after each electrolysis. Immersion in the HCl solution for more than 3 hours may cause surface etching and should be avoided. The gas dispersion tube from the catholyte chamber should be cleaned in a concentrated HCl solution (20 vol.%) overnight. After cleaning, there should be no residual acid solution on the cell body and the gas dispersion tube, which should be thoroughly rinsed with D.I. water to avoid changes in the reaction environment during electrolysis.

Ensuring an airtight electrolysis system is crucial for accurate quantification of gas products and precise evaluation of catalyst activity coupled with current density. To achieve a leak-free system, it is necessary to tighten bolts and nuts with evenly distributed torque, securing each component and balancing the pressure throughout the cell. A digitized torque wrench is recommended for assembling the components, applying a torque of 4.10 in-lb. It is important not to overtighten, as this can lead to thread deformation, tube cutting, or cracking of the cell body materials.

Additionally, proper preparation of O-ring surfaces should be considered. In the laboratory's batch-type electrolyzer, Viton O-rings are used. These polymer-based O-rings are chemically inert and help ensure airtightness through concentrated force along the perimeter. However, if the surface of the O-rings is cracked or contaminated, it can be a source of leaks. To prepare a clean surface, ultrasonication in D.I. water for at least 20 minutes, followed by rinsing with IPA solution, is required before use. Cracked O-ring surfaces should be replaced with fresh ones.

The membrane should be cut to fit the area between the anolyte and catholyte chambers. The total membrane area should cover the O-ring but not reach the screws. Before assembling the cell, the membrane should be rinsed thoroughly with D.I. water. After rinsing, it is necessary to perform ultrasonication in D.I. water for 20 minutes, followed by rinsing with D.I. water again. The cleaned membrane should be stored in D.I. water unless it is immediately used for the next CO_2 electrolysis.

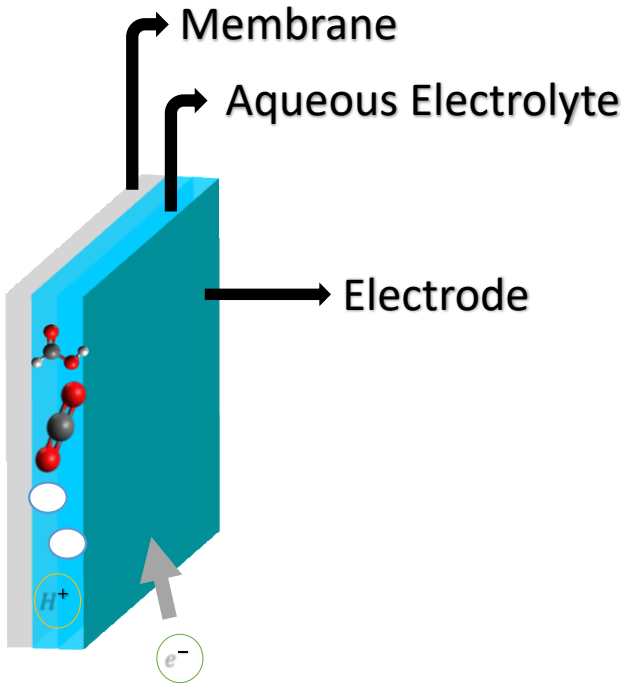

Figure 1.6. Schamatic of a batch cell (H-Cell) setup.

1.3.2 Zero gap MEA Flow Cell Electrolyzer:

The customized membrane electrode assembly (MEA) type electrolyzer from Fuel Cell Technology, Inc. is designed to improve the overall performance of the CO_2 conversion system by facilitating rapid mass transport of CO_2 to the catalyst sites. To optimize the electrolyzer design for liquid products, particularly formate in this thesis, a zero gap MEA electrolyzer is developed based on benchmarking the membrane-electrode-assembly type electrolyzer used in water electrolysis and fuel cell applications.

The zero gap MEA electrolyzer sandwiches the gas diffusion electrode (GDE) with a flow field and a membrane. A cation exchange membrane, specifically Nafion 117 from Fuelcellstore, is used to facilitate proton transport from the anode chamber to the cathode chamber through diffusion across the membrane. The direct contact between the catalyst layer and the membrane helps maintain the ohmic resistance of the electrolyzer at around 3 ohms. The Nafion membrane is pre-cut to a size of 1.8×1.8 cm^2 and stored in the anolyte for at least 12 hours prior to electrolysis after undergoing 20 minutes of sonication in deionized (DI) water.

An interdigitated flow pattern is employed to ensure well-distributed CO_2 feed and anolyte circulation within the electrolyzer. A sodium phosphate buffer solution with a concentration of 0.5 M and pH of 3 is used as the anolyte, which is circulated using an analogue peristaltic pump. Graphite and titanium (Ti) are chosen as materials for the cathodic and anodic flow field, respectively, considering their standard reduction potential as indicated by the Pourbaix diagram.

The gas products and liquid products at the interface between the membrane and the catalyst layer are diffused out from the GDE. The electrolyzer is made airtight using polytetrafluoroethylene (PTFE) gaskets and O-rings. The gaskets have a window to accommodate a 1×1 cm^2 area of the GDE. An IrO_x-coated Ti mesh is utilized as the anode, while gold-plated thin metal plates serve as current collectors. All the components are clamped together using end plates.

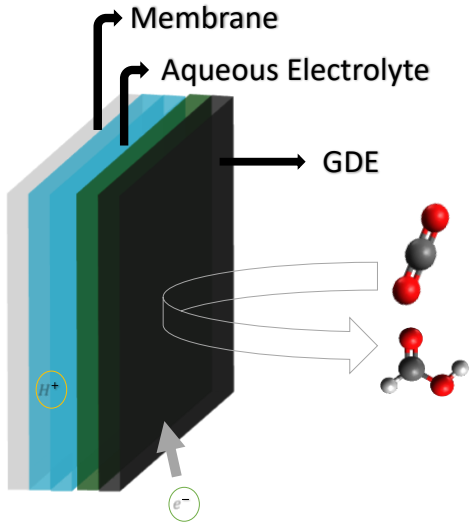

Figure 1.7. Schematic of a MEA electrolyzer setup

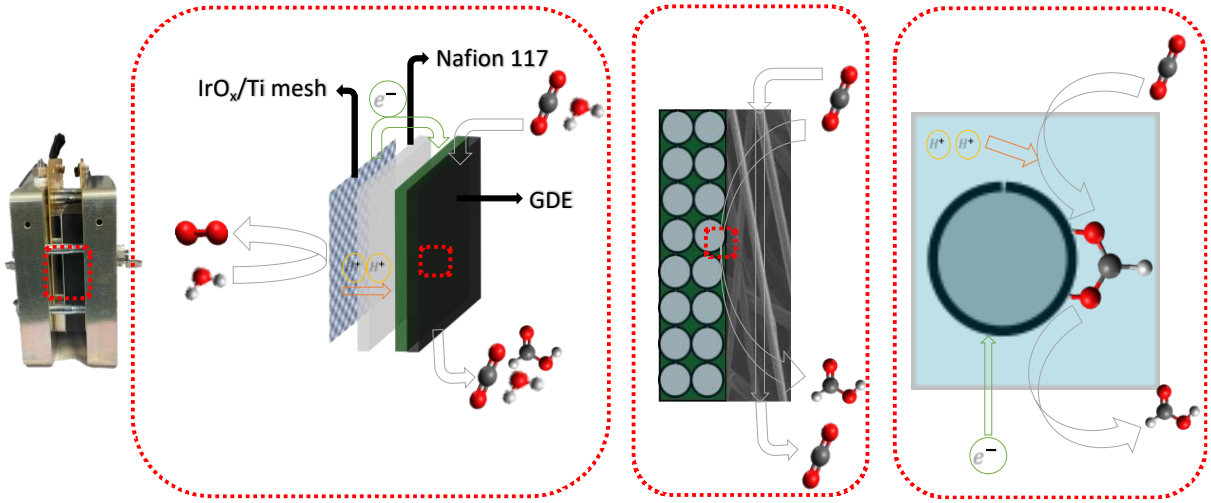

Figure 1.8. Mechanism of CO_2 reduction to formic acid in a Zero-gap MEA electrolyzer setup

1.4 Quantification of CO_2RR products

Efforts have been made to quantify both the gas and liquid products generated in the CO_2 electrolysis system. The expected gas products include CO, hydrocarbons such as CH_4, C_2H_4, and C_2H_6, and parasitic H_2. On the other hand, the liquid product in the interest of this thesis research is formate,

The gas products are formed on the catalyst surface and are simultaneously collected in a sampling loop connected to a gas chromatograph (GC). The GC used is an SRI GC 8610C. The gas samples (1 ml) are collected from the inner loop of the GC, and an unreacted CO_2 gas stream is used as a transport medium to transport the samples into the GC columns. Argon (Ar) carrier gas, at a pressure of 15 psi, is then used to further carry the sample gases through the columns in the oven. The temperature range of the oven is set between 50°C to 90°C. A molecular sieve 5A column is employed to separate hydrogen (H_2), while a haysep D column is used to separate CO, CH_4, C_2H_4, and C_2H_6. Detection of H_2 is done using a thermal conductivity detector (TCD), and detection of CO, CH_4, C_2H_4, and C_2H_6 is done using a flame ionization detector (FID). CO detection is achieved using a methanizer, which is equipped with the FID (the separate H_2 gas pressure to the methanizer is set to 20 psi). To ensure repeatability and monitor catalyst activity over the electrolysis time, online quantification is performed four times within an hour of CO_2 electrolysis. Prior to CO_2 electrolysis, the GC is calibrated using a mixed gas containing specified concentrations of CO, CH_4, C_2H_6, H_2, C_2H_4, CO_2, oxygen, and nitrogen, balanced with Ar. Additionally, the GC columns are baked at 250°C on a weekly basis to remove any residue compounds.

As for the liquid products, they accumulate in the catholyte chamber (batch-type reactor) and the liquid product reservoir (zero gap MEA electrolyzer) during the electrolysis. These liquid products are sampled at the end of the electrolysis to ensure the airtightness of the electrolyzer. To quantify the liquid products, two instruments of ^1H nuclear magnetic resonance (NMR) are

utilized (specifically the ECA500 model from JEOL). A pre-saturation step is performed during the NMR analysis to suppress the water peak by using a presaturation power of 50 dB.

Chapter 2

Modulating proton availability on the Copper sulfide surface to improve the selectivity of CO_2 electroreduction to Formate

2.1 Introduction

Among the different types of greenhouse gases, CO_2 is of greatest concern due to its contribution to the most enhanced greenhouse effect and climate change. Energy-driven consumption of fossil fuels has led to a rapid increase in CO_2 emissions which resulted in disruption of the global carbon cycle. As a result, global atmospheric CO_2 concentration has increased by more than 20% to 420.1 ppm Among all greenhouse gases, like methane, nitrous oxides, and fluorinated gases, carbon dioxide retains less heat than the others. However, carbon dioxide accounts for around 82% of GHG emissions, so the sheer quantity of CO_2 being released into the atmosphere by humans every year makes it one of the leading instigators of climate change. Common anthropogenic sources of atmospheric carbon dioxide include industrial processes, like refineries, chemicals production, cement industry; coal-fired power plants; and transportation sector. To limit this aggravatingly increasing concentrations of CO_2, various carbon capture, storage and utilization processes have been developed. Among which electro-reduction of CO_2 has caught the eye of

various scientists and researchers because of its ability to generate value by producing value added fuels and chemicals.

CO_2 electro-reduction produces various carbon-based fuels and chemicals ranging from $2e^-$ products such as carbon monoxide and formic acid to 18 e^- product such as 1-propanol. As discussed in chapter 1, the CO_2RR mechanism on the catalyst proceeds via either *COOH adsorption or *OCHO adsorption. The former produces carbon monoxide and other hydrocarbons and oxygenated carbonaceous species. Due to its intrinsic catalytic behavior, Copper has been known to generate 16 products and fuels [8], majority of which proceeds via *COOH intermediate.

Due to the unique *OCHO intermediate pathway, formate is a minor product when catalyzed by copper alone. However, there have been some studies [9,10] where the authors tweaked the copper material by introducing a partial positive local environment by forming copper sulfide. Due to the partial positive local environment, the affinity of CuS to bind with oxygen is thereby improved and hence the formation of formate proceeds through downhill reaction coordinate [11] as opposed to uphill in the case of Cu (111) surface.

Another important factor in efficient CO_2 reduction to formate is the availability of proton for the reaction to progress. In this lieu, a study conducted on gold [12], which predominantly produces CO, revealed 20% production of formate through the introduction of ligands where their pKa determined the relative order of faradaic efficiency. The higher the pKa, the lower the ability of the ligand to dissociate and form proton, thereby lowering the ability of the catalyst to produce formate. However, on the other side, if the pKa value is lower, there are a lot of protons available in the catalyst environment which led rise to increase in parasitic hydrogen evolution reaction. Thereby, an optimum pKa ligand is required to steer the reaction in favor of formate production.

This prompted us to study the effect of ligands and modulate the chemical environment on CuS for effective production of formate. The ligands chosen in this study in the order of pKa are 3 Mercaptopropionic acid (pKa -COOH = 4), 2 Mercaptoethanol (pKa -OH = 16), and Ethanethiol (pKa -CH_3 = 50). We expect 2 Mercaptoethanol to give the highest faradaic efficiency towards formic acid. Figure shows the plot of the anticipated trend using the above ligands and the argument.

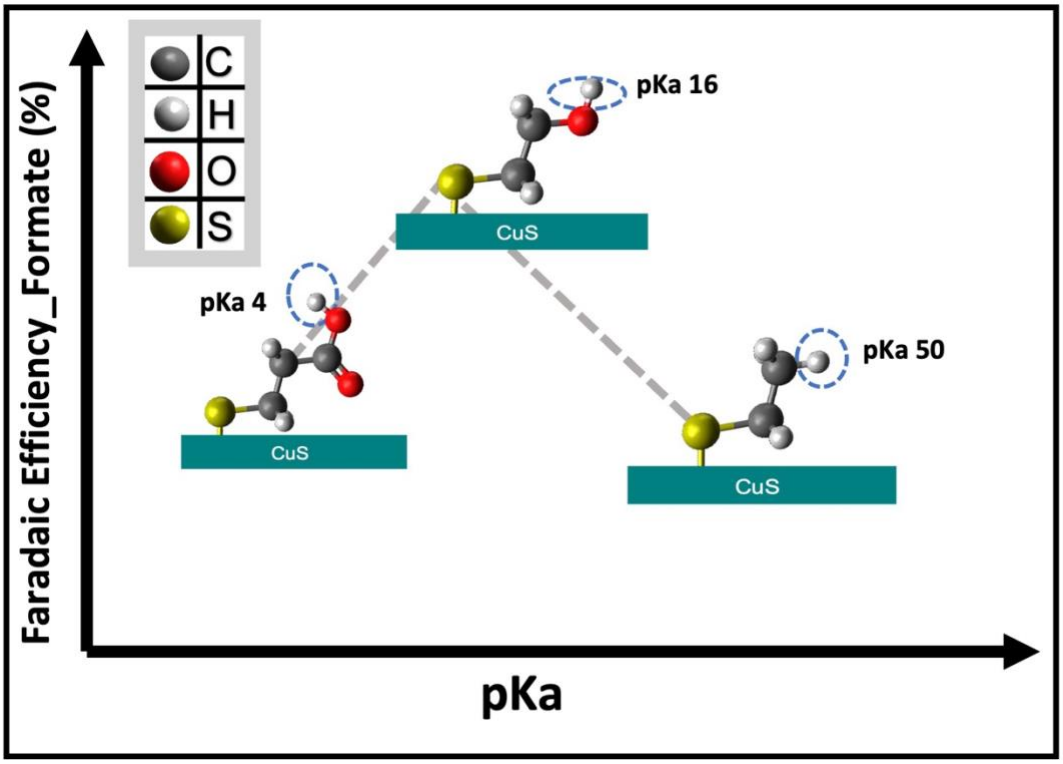

Figure 2.1. Expected trend of various ligands capped on CuS surface based on their pKa values.

2.2. Experimental Procedure

2.2.1 Synthesis methods:

Copper sulfide capped with Oleylamine:

The preparation process is a modified version of the work done by Zeng et. al. [13] 165.6 mg of copper (II) nitrate hemi pentahydrate is added to 4 mL OLAM

and 12 mL 1-octadecene and sonicated. 76.8 mg of sulfur powder is added to this solution in a 50 mL round bottom flask. The mixture is heated at 160 C for 33 min in a silicone oil bath. The solution is then allowed to cool, and 16 mL ethanol is added before centrifuging at 3500 rpm for 7.5 min. The wash solution was removed, and the precipitate was redispersed in chloroform and ethanol for centrifugation. This wash process was repeated one more time and the solution was dissolved into 4 mL chloroform.

Ligand exchange:

To perform the ligand exchange, 1.5 mL of ethanol and 0.5 mL of 3 Mercaptopropionic acid or 2 Mercaptoethanol is added to 1.5 mL of the Copper Sulfide capped with Oleylamine to obtain Copper Sulfide capped with 3 Mercaptopropionic acid and 2 Mercaptoethanol, respectively. For the Ethanethiol ligand exchange 1 mL of 5 vol% Ethanethiol in ethanol is used.

The ligand exchange solution is stirred for 1 day. The solution is then centrifuged, and the precipitate is redispersed in chloroform and ethanol, and centrifuged again. Post this step, the precipitate is redispersed in 1.5 mL of ethanol and 1.5 mL of chloroform and then stirred for 1 day with either of 0.5 mL of 3 Mercaptopropionic acid or 0.5 mL of 2 Mercaptoethanol, or 1 mL of 5 vol% Ethanethiol, respectively. The solution is then centrifuged, and the precipitate is redispersed in chloroform and ethanol for a total of three centrifugation steps. The final precipitate is redispersed in chloroform for Langmuir Blodgett assembly or ethanol for ink preparation to coat on the Glassy Carbon Disk.

2.2.2 Electrode preparation

Glassy Carbon Electrode polishing

The glassy carbon electrodes' surface was mirror polished using a combination of alumina slurry, nylon, and micro cloth fabric (purchased from pine research). The glassy carbon was wiped with ethanol and de-ionized (type 1) water using a clean room wipe to ensure there are no traces left behind on the surface. A single drop of 5µm alumina slurry was poured on a nylon cloth and the glassy carbon disk was polished in the shape of 8 curve for about 5 minutes which was then followed by pouring a single drop of 0.3µm alumina slurry on a micro cloth fabric for about 10 minutes followed by 0.05 µm alumina slurry on a micro cloth fabric for about 15 minutes. The glassy carbon disk was rinsed and put in a bath sonicator with de-ionized water after each of the above steps to ensure mirror finishing.

Coating catalyst onto the glassy carbon disk

Traditionally, most of the fundamental catalyst study involving a glassy carbon disk proceeds through a formulation of ink [14,15,16,17] and drop casting the ink onto the glassy carbon disk using a nafion binder and allowing the solution to evaporate to yield the particles coated on the glassy carbon disk. The evaporation rate is modulated by the alcohol % in the ink solution prepared.

However, due to the addition of nafion, it disturbs the uniformity and morphology of the synthesized species which makes it difficult to analyze the observing parameters. Owing to this non-uniformity, we proceeded with an alternative approach to

coat the catalyst onto the glassy carbon disk by making use of the relative hydrophobicity of the ligands on CuS and the Langmuir Schaufer process.

The nanodisks were dispersed in chloroform. The dispersion was dropped onto the air-water interface of a KSV NIMA Langmuir–Blodgett trough. As the chloroform evaporated, a dilute layer of nanodisks was left on the interface. The layer was compressed using teflon barriers to a surface pressure of 14 mN/m. The film was transferred to a glassy carbon electrode using the Langmuir-Schaefer method as depicted in the figure 2.2.

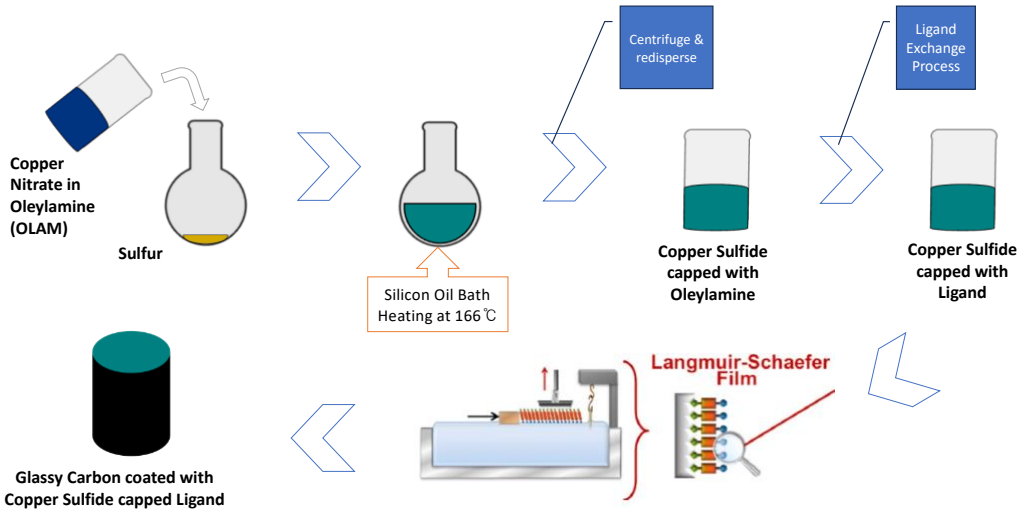

Figure 2.2. Schematic description of the synthesis process

Figure 2.3 show the scanning electron microscopy (SEM) images of these single coated copper sulfide particles. The SEM images were taken using the instrument FEI FESEM Apreo, Nano3. The SEM images reveal slight agglomeration of particles in the case of 3 Mercaptoprionic acid and 2 Mercaptoethanol due to their relative hydrophilic nature.

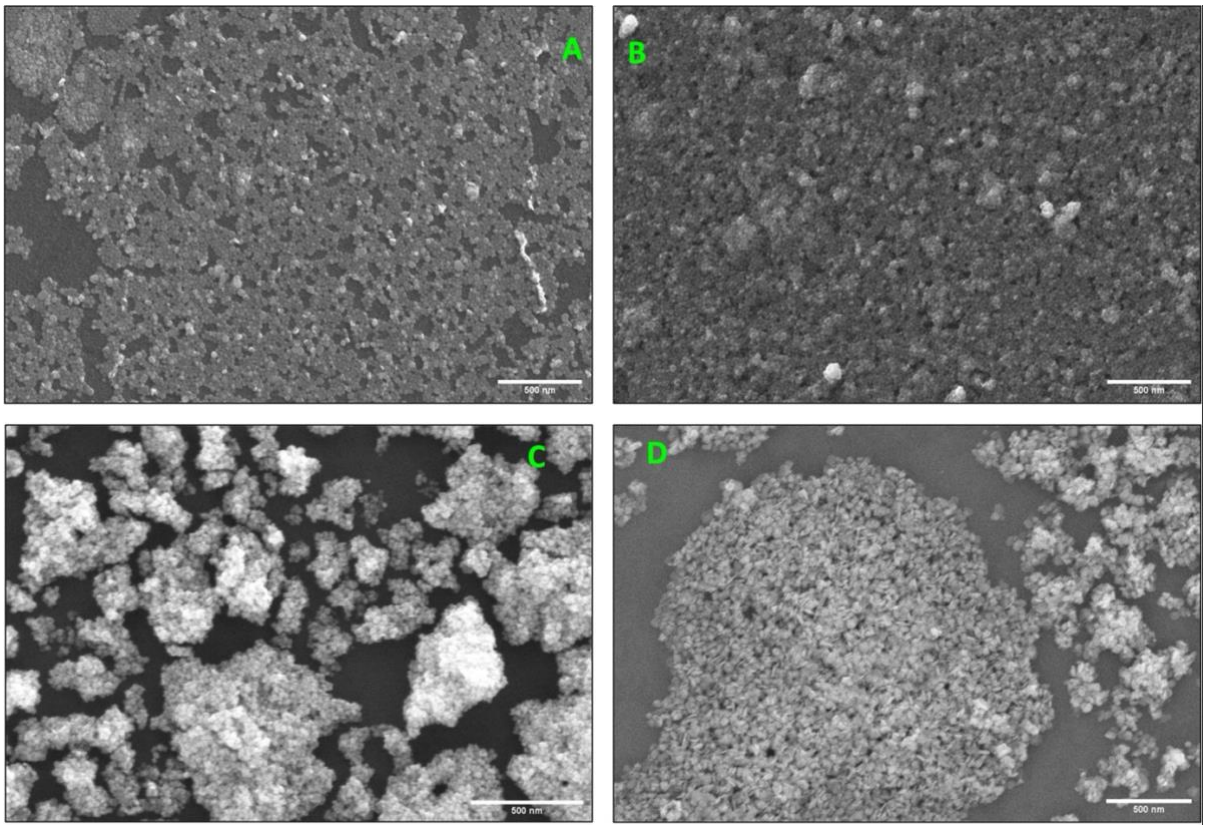

Figure 2.3. Scanning electron microscopy (SEM) images of Copper Sulfide capped with (A) Oleylamine, (B) Ethanethiol, (C) 2 mercaptoethanol, (D) 3 mercaptopropionic acid coated on the glassy carbon disk using the Langmuir Schaefer process.

Figure 2.4 reveal the FTIR and UV-Vis-NIR spectroscopy data for these ligands exchanged copper sulfide material. FTIR spectra were taken using a Nicolet iS50 Fourier transform infrared (FTIR) spectrometers in transmission mode by through nanoparticles drop casted on a KBr window. For Oleylamine, the peaks at 1457 cm^{-1} represent CH_3 and 1593 cm^{-1} represent NH_2. [18] 3 Mercaptopropionic acid has the large double peaks as the $v_{sym(COO)}$ and $v_{asym\ (COO)}$ which is validated with this [19]. Ethanethiol doesn't have any characteristic peak distinguishable from OIeylamine. However due to the strong peak at around 2900 cm^{-1} which represent the CH_2 molecule, we can best assume that is the identifying peak for Ethanethiol. 2 Mercaptopropionic acid has a double peak around 1000 cm^{-1}, however the OH peak around 3300 cm^{-1} would have been the best identifier. [20,21]

UV-Vis-NIR spectra were taken using a Perkin Elmer Lambda 1050 UV/VIS/NIR spectrophotometer. Measurements were taken in chloroform with a 1 cm quartz cuvette. The sharp peak is from the background which is completely absorbing in that region. We speculate it to be $CHCl_3$.

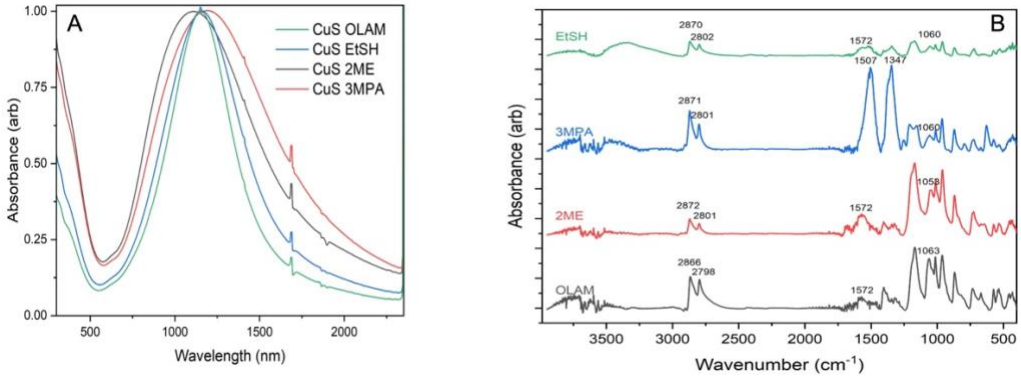

Figure 2.4. UV-Vis-NIR spectroscopy (A) and FTIR spectroscopy (B) of Copper Sulfide capped with Oleylamine, 3 Mercaptopropionic Acid, 2 Mercaptoethanol, Ethanethiol coated on the glassy carbon disk using the Langmuir Schaefer process.

The loading on the glassy carbon disk were estimated to be 24.0 $\mu g/cm^2$, 17.0 $\mu g/cm^2$, 3.9 $\mu g/cm^2$ and 2.86 $\mu g/cm^2$ for 3 Mercaptopripionic acid, 2 Mercaptoethanol, Ethanethiol and Oleylamine, respectively. These glassy carbon disks with the above loading were used to study the electrochemical reduction of CO_2.

2.2.3 Carbon Dioxide electrolysis

The CO_2 electrolysis is carried out in a custom-made H-cell using a three-electrode setup at room temperature and ambient pressure. Graphite Rod (pine research) and Ag/AgCl (in KCl gel, pine research) constitutes the counter and reference electrodes respectively. Copper tape is put on the glassy carbon to improve the conductivity throughout the circuit. The working

and counter electrode compartments are separated by an anion exchange membrane (Selemion AMV, AGC inc.). Research grade CO_2 is continuously purged at a flow rate of 5sccm, controlled via a mass flow controller (Smart Track 100, Sierra) into an aqueous purified electrolyte made of 0.7 M $KHCO_3$ solution (≥ 99.95% metal basis, Sigma-Aldrich), pH = 7.6. The purification of electrolyte is done using a chelating agent (Chelex 100, Bio-Rad Laboratories, Inc.) to remove any metallic impurities. The system is purged 30 mins to reach the CO_2-solubilized electrolyte condition before any electrochemical analysis is done. The electrochemical analysis of the electrodes is conducted using a potentiostat (VSP-300, biologic). The potentials reported are corrected by 85% automatic iR-compensation and 15% manual compensation and converted to the reversible hydrogen electrode (RHE) scale. Prior to 1hr CO_2 electrolysis, the surface of the catalyst coated glassy carbon undergo pre-electrolysis for 10 min at the corresponding potentials to remove the native oxide layer.

2.2.4 Products quantification

All gas products produced in the catholyte chamber travel through a network of tubing to the gas chromatograph (SRI 8610C GC) and quantified by online gas chromatography with a molecular sieve 5A and a Haysep D column, a TCD/FID detector, and using Ar as a carrier gas. During 1hr of chronoamperometry experiments, 4 online injections happen to the GC and the current density is averaged at these 4 injection times. The liquid products from both catholyte chamber and anolyte chamber (total volume of the cell: 12.720 ml) are quantified at the end of the electrolysis using ^1H nuclear magnetic resonance (NMR) spectroscopy with a 500 MHz spectrometer (ECA500, JEOL) where the water peak was suppressed using a presaturation irradiation at 50 dB.

Geometric partial current density of the products is computed using the data from steady state current density chronoamperometry experiments and quantification of the products by the

TCD/FID channels of the gas chromatograph and ^{1}H NMR for the liquid product, essentially formic acid.

2.3. Effect of applied potential

The single coated Oleylamine (OLAM) capped CuS glassy carbon electrode was used in a custom designed H-Cell as the working electrode with graphite rod (pine research) and Ag/AgCl, KCL gel (pine research) being the counter and reference electrodes respectively. All the potentials reported in this section are referenced to the reversible hydrogen electrode (RHE) and iR compensated, 85% by the biologic potentiostat and 15% manual correction. The reactions were carried out at -0.5 V, -0.6 V, -0.7 V and -0.9 V (vs) RHE to observe the trend with the applied potential. Figures represent the faradaic efficiency data vs applied potential. The faradaic efficiency is maximum at -0.6 V (vs) RHE with 35.7% faradaic efficiency towards formic acid. As the reduction potential bias is increased to -0.7 V (vs) RHE and -0.9 V (vs) RHE, CO, CH_4 and other carbon products are observed which is an indication that the surface is reduced to elemental copper instead of the partially positively charged copper species. The onset potentials for the above carbon species are matched with the literature values to confirm the presence of elemental copper. Henceforth, -0.6 V (vs) RHE was chosen as the working potential to study the effect of ligands.

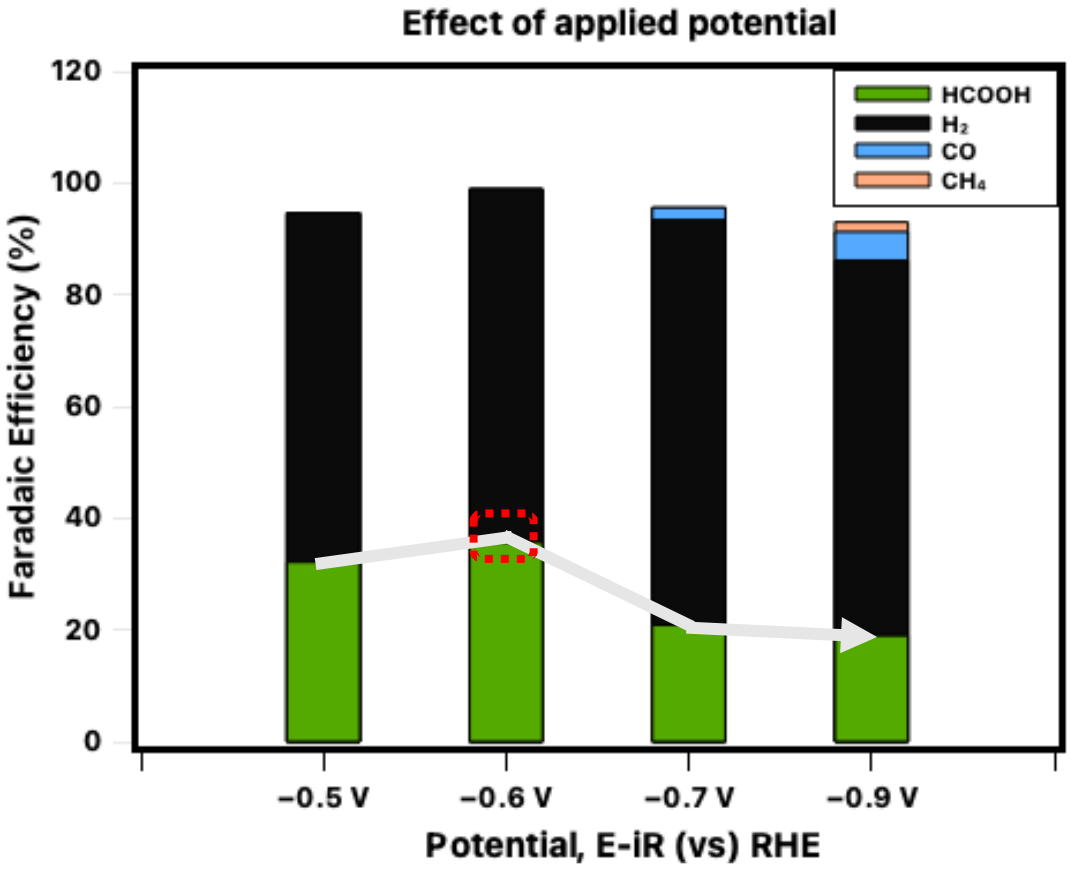

Figure 2.5. Effect of applied potential on the Oleylamine capped single coating glassy carbon electrode. The potentials are corrected for iR compensation and are referenced to the reversible hydrogen electrode (RHE).

2.4. Effect of ligands and their pKa

Copper sulfide capped with Oleyl amine goes through a ligand exchange to obtain copper sulfide capped with 3 Mercaptopropionic acid (3MPA), 2 mercaptoethanol (2ME), and ethanethiol (EtSH) as desired to study the effect of their pKa towards the activity and selectivity of formic acid for the CO_2 electroreduction. Figure shows the plot of faradaic efficiency (vs) ligands in their order of pKa. The plot is in line with the hypothesis explained earlier in this chapter, which confirms that an optimal pKa ligand is required to promote the production of formic acid. The formic acid is

produced with $70.15 \pm 1.77\%$ faradaic efficiency over the 2 mercaptoethanol (pKa = 16) capped on copper sulfide.

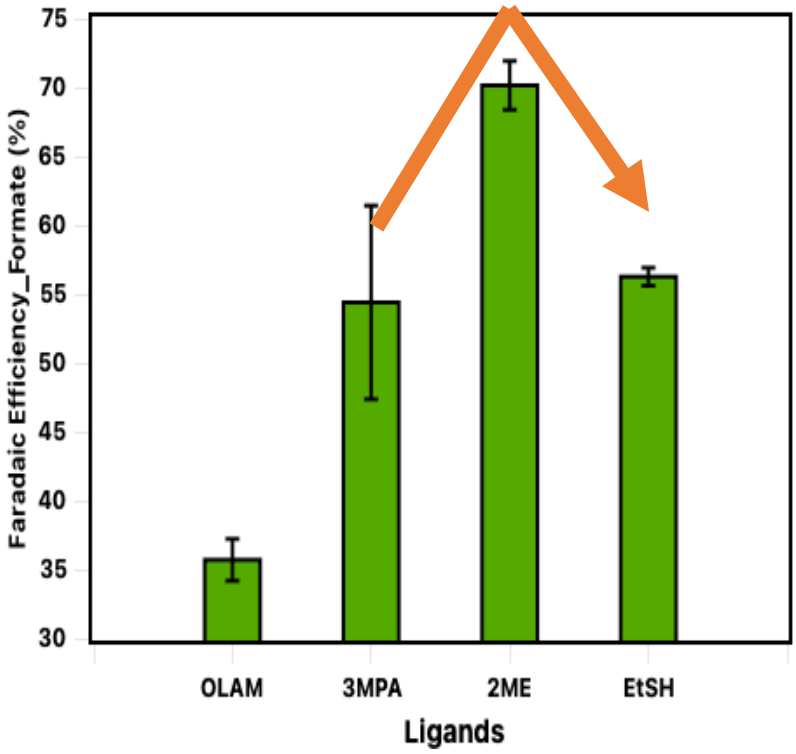

Figure 2.6. Effect of ligands and their pKa on Faradaic efficiency of Formate. The chronoamperometry was performed at iR compensated -0.6 V (vs) RHE. The liquid product, formic acid, was characterized using ^{1}H NMR spectroscopy. The error bars represent the standard deviation among the repeated experiments.

Figure 2.7 show the plots of cyclic voltammetry performed at scan rates of 20 mV/s, 40 mV/s, 60 mV/s, 80 mV/s and 100 mV/s. According to the theory, the current is proportional to the scan rate, with the Electrode Double Layer Capacitance (EDLC) of the electrode being the proportionality constant. The Electrochemical Surface Area (ECSA) was determined by taking the ratio of the above capacitance (EDLC) with that of pure crystalline copper (0.03 mF/cm^2). The formate partial current density normalized to ECSA is 80% higher for 2 mercaptoethanol capped copper sulfide among the other ligands due to its optimum pKa.

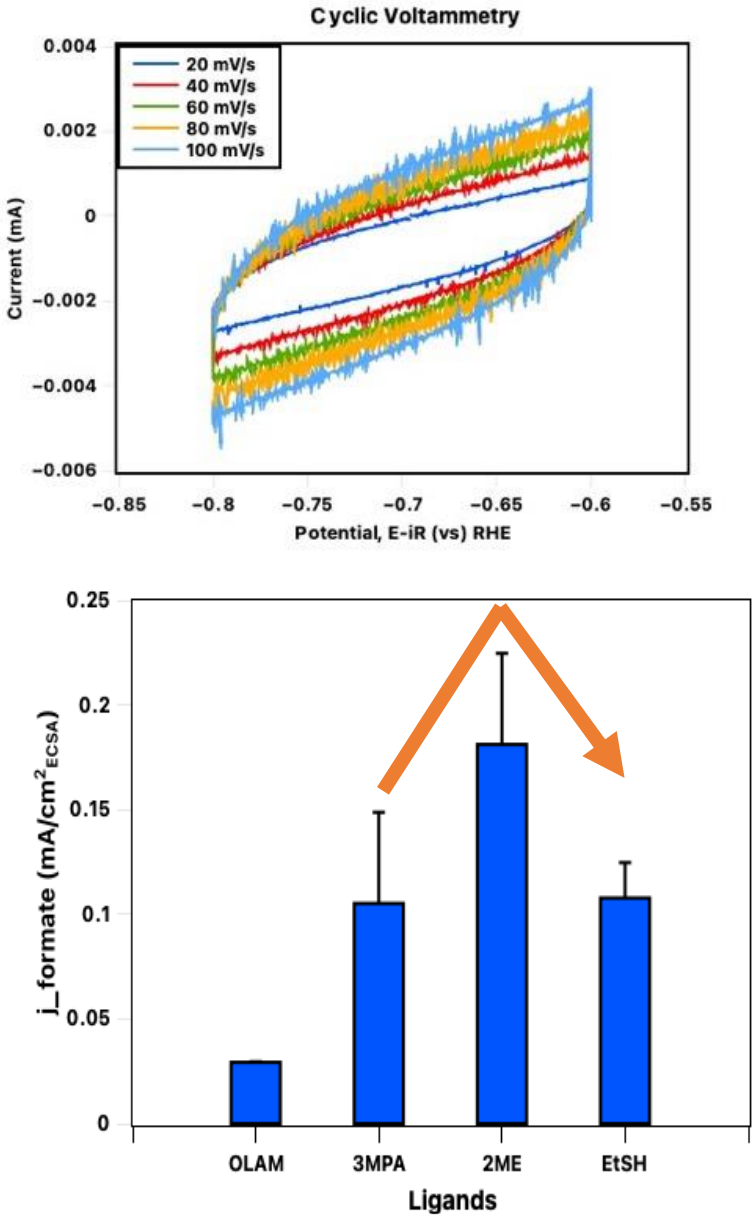

Figure 2.7. (A) Cyclic Voltammograms performed at scan rates ranging from 20 mV/s to 100 mV/s for the potential window -0.6 V to -0.8 V (vs) Ag/AgCl to evaluate the Double Layer Capacitance and ECSA. **(B)** Partial current density of Formate normalized by ECSA for the copper sulfide capped with ligands decided based on their pKa values. The error bars represent the standard deviation among the repeated experiments.

2.5 Summary

CO_2 electrocatalytic reduction to formate activity and selectivity are governed by the stabilization of the *OCHO intermediate which is possible by using a partial positively charged copper species on the surface as that of copper sulfide. The ligand plays a key role in supplying the proton required for the reduction of CO_2 to formate, and that an optimum pKa value ligand is beneficial owing to the arguments made above.

Figure 2.8 compares the faradaic selectivity of the state-of-the-art catalysts in an H-Cell system for the given potential range. Among the copper sulfide study, our data reports 70.15% faradaic efficiency which is about 25% higher than the previously reported value in the literature [10,22,23,24,25,26,27] at -0.6 V (vs) RHE, which highlights the importance of chemical environment of the catalyst species in aiding the production of formate.

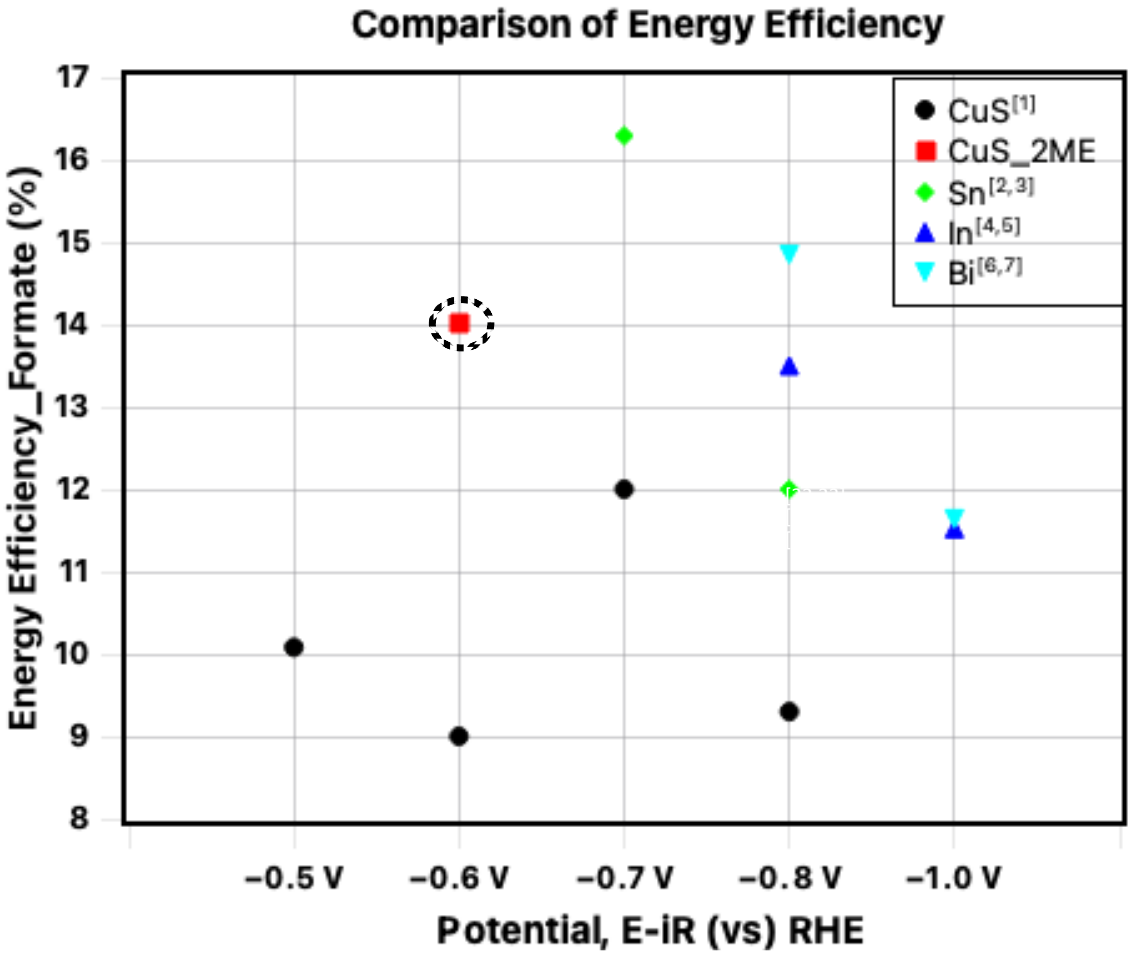

Figure 2.8. Comparison of faradaic efficiency of our catalyst with the state-of-the-art catalysts in the H-Cell based electrolyzer.

However, there are a few questions that arise in this work. Some of the main questions are if the ligands were completely exchanged. Since we observe a few peaks corresponding to Oleylamine in the FTIR spectrum of 2 mercaptoethanol, 3 mercaptopropionic acid and ethanethiol it is an indication of some oleylamine present on the surface.

Another question that comes in about using longer chain ligands with different pKa values. However, the longer chain ligands come at the cost of inhibition of CO_2 from accessing the active site as well as poor conductivity of the long chain carbon species on the ligand. Among the short chain ligands that were studied here, a few more intermediate pKa based ligands can be studied to get an overall idea and touch base on the optimum pKa conditions. Nonetheless, this work provides with promising data towards the optimal pKa conditions based on the three ligands chosen in this study.

Figure 2.9 show the post electrolysis SEM image of the catalyst. We observe that the catalyst got aggregated on top of the glassy carbon electrode. Raman analysis on the material direct towards copper oxide on the surface. This questions the stability of the material under the electrochemical environment.

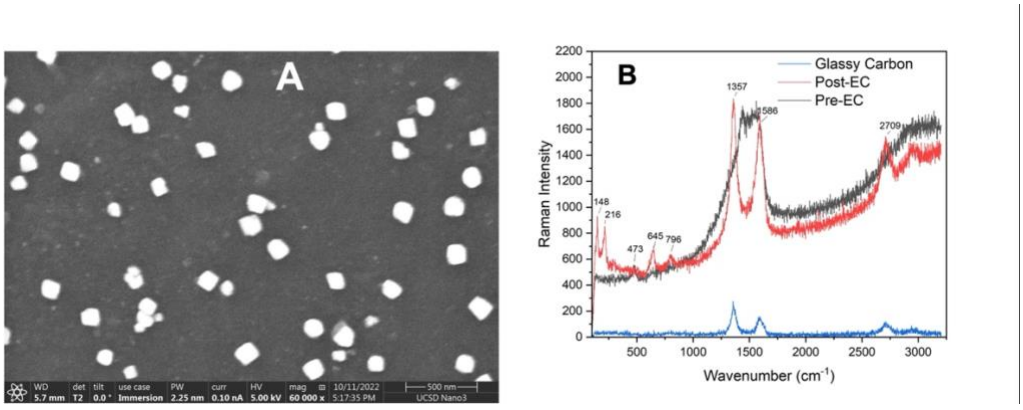

Figure 2.9. (A) Post electrolysis SEM image of the glassy carbon electrode. **(B)** Raman analysis on the material pre and post electrolysis and its comparison with a polished glassy carbon disk with no material. The peaks corresponding to Pre-EC 467 cm^{-1} come from S-S bonds in CuS. Post-EC 148 cm^{-1} and 216 cm^{-1} indicates Cu_2O. 1357 cm^{-1}, 1586 cm^{-1}, and 2709 cm^{-1} are peaks for the glassy carbon.

Nevertheless, this work brings in novel approaches to engineer the catalytic environment of the catalyst and a non-conventional coating technique on to the glassy carbon substrate. The

results shown in this study is a promising indication of the tuning the micro-environments to steer the chemistry in desired direction.

Chapter 3

Tuning the Oxidation State of SnO_x and Mass Transport to Enhance Catholyte-Free CO_2 -to-Formate Electrolysis

3.1 Introduction

The electrochemical reduction of carbon dioxide to valuable chemicals has gained significant attention due to its crucial role in addressing climate change and the energy cycle. The electrochemical recycling of waste CO_2 presents an opportunity for large-scale storage of renewable electricity in the form of chemical bonds. Among the various electrochemical CO_2 conversion products with added value, formic acid is particularly intriguing for achieving net negative carbon emissions, as its synthesis requires less electrons compared to the production of multi-carbon compounds. Formic acid is also known to be a hydrogen carrier which enables its potential in direct formic acid fuel cells.

Among the transitional metals, tin is one of the attractive metals for electrochemical CO_2 reduction to formic acid. Due to its optimal binding energy with *OCHO intermediate [28], it suppresses the reaction path toward CO, hydrocarbon, or alcohols since the latter proceeds via *COOH intermediate. Oxide derived tin have shown improved activity [29] and selectivity towards formic acid. Within the oxide derived state, a catalyst with SnO and SnO_2 present on its surface shows improved faradaic efficiency towards formic acid as compared to metallic tin. [30] Despite various fundamental studies of CO_2 reduction to formic acid on mixed tin oxide surface, the industrial feasibility is still in question because of lack of integration of fundamental sciences and engineering a practical electrolysis system.

Within the ecosystem of fundamental studies of CO_2RR, majority of the work was focused on dissolving CO_2 in aqueous electrolyte and then perform electrochemical analysis. This limits the current because the CO_2 is sparingly soluble in aqueous electrolyte. [31] which limits its potential application in large scale industries where a high current density is desired. Researchers over the time have come up with a system to utilize the Gas Diffusion Layer (GDL) to eliminate the need to solubilize CO_2 and enable direct feed of gaseous CO_2 to the electrode surface where catalyst layer and electrolyte are present. [32,33]

Talking from a separations point of view, the liquid CO_2RR products get diluted within the catholyte which incurs additional separation costs to purify the products. Because of which a zero-gap MEA electrolyzer was introduced where the limitation of dilution of liquid products is overcome which is a promising solution from industrial point of view and require more experimental studies [34,35,36,37].

This study focusses on the application of a zero-gap MEA electrolyzer to effectively convert CO_2 to formic acid using electrochemical pathways and addressing the importance of mixed chemical state of tin, effect of CO_2 concentration and flow rate, and concluding the study describing the mass transport phenomenon.

3.2 Experimental Procedures

3.2.1 Electrode preparation

To fabricate electrodes made of Sn oxides, SnO_2 nanoparticles (99.7% purity, 35-55 nm, sourced from US Research Nanomaterials) are placed inside an alumina-coated tungsten boat within a high vacuum chamber (pressure below $7x10^{-7}$ mTorr) for thermal evaporation. The deposition rate is maintained at 0.14-0.2 A˚s−1 onto the cut 1cmx1cm

Gas Diffusion Layers (GDLs), which were obtained from Fuelcellstore (AvCarb GDS2230). The thickness of the tin oxide layers is monitored using a quartz crystal microbalance (QCM).

The as-prepared electrodes undergo post-heat treatment by annealing them at 300℃ for 5 hours in a muffle furnace. The surface morphology of the as-prepared electrodes is examined using scanning electron microscopy (SEM, Zeiss, Sigma 500). The surface valence band and core-level electronic structure of the electrodes are analyzed using X-ray photoelectron spectroscopy (XPS) with a 90° emission angle relative to the electrode surface (Kratos, AXIS Supra) under vacuum conditions below 5×10^{-8} Torr. XPS spectra are recorded with pass energies of 160 eV for the survey scans and 20 eV for the narrow scans. The binding energies are calibrated using both the Fermi edge (0.06 eV) and the Au 4f7/2 second-order peak (84 eV).

For the preparation of IrO_x anodes, a modified thermal pyrolysis method is employed [38,39]. Surface-etched titanium meshes (purchased from Fuelcellstore) are used as substrates. The meshes are cut into 1 cm^2 pieces and subjected to sonication in a mixture of acetone, IPA, and DI water (6:3:1 v/v), followed by rinsing with DI water for 10 minutes each. The cleaned substrates are etched in a 20% HCl solution for 5 minutes, then transferred to a boiling 10% oxalic acid solution for 10 minutes, and finally cleaned with DI water using bath sonication. A precursor solution is prepared by dissolving 26 mg of Iridium (III) chloride hydrate (99.9% purity, obtained from Sigma Aldrich) in a mixture of 6.71 ml IPA and 2 ml of concentrated HCl solution. The precursor solution is then dropped onto the surface-etched titanium meshes, which are preheated to 125℃, until a total loading of 1.0 mg cm^{-2} is achieved. The electrodes are subsequently annealed at 500℃ for 3 hours in a muffle furnace. The contact angles of water (H_2O) on the electrodes are measured using a Goniometer (rame-hartTM Model 200). The crystalline structure of

the tin oxide electrodes is analyzed using X-ray diffractometry (XRD, Rigaku, Smartlab) with a parallel beam configuration.

3.2.2 Electrolyzer Configuration:

A customized zero-gap electrolyzer purchased from Fuel Cell Technologies, Inc with an active area of 1 cm^2 was used for all CO_2 electrolysis along with the interdigitated flow channels on graphite and titanium current collectors for cathode and anode, respectively. PTFE sheets (0.01 inch) were used as gaskets to block the leak of any gas. After rinsing and sonicating the Nafion 117 membrane with DI water and soaking the same in the anolyte solution for overnight, it was utilized as a membrane due to its intrinsic ability to transport protons from the anode section of the cell to the cathodic surface. The above prepared IrOx/Ti were used as an anode for its exceptional performance for the Water Oxidation Reaction. In the end, the electrolyzer is tightened using 8 hex screws sequentially torqued (8-10-12 Nm) with a digital torque wrench.

3.2.3 CO_2 Electrolysis:

Electrochemical analysis is conducted in a two-electrode system using a potentiostat (VSP-300, biologic). The prepared cathodes, Nafion membrane, and IrOx/Ti anode are arranged and compressed together with PTFE gaskets, current collectors, bipolar plates and end plate. A solution of 40 ml 0.5 M sodium phosphate buffer (98% purity, Fisher Scientific) with a pH of 3 is circulated through the titanium flow channels on the anode side as the anolyte, utilizing a peristaltic pump. Research-grade CO_2 gas is supplied to the graphite flow channels on the cathode side through a custom-made bubbler humidifier setup, with a flow rate of 200 sccm, unless stated otherwise. The flow rate is controlled by a mass flow controller (Smart Track 100, Sierra and Newport MFC G series). The partially concentrated CO_2 stream (3%, 15%, 40% and 70% CO_2) is prepared by balancing it with research-grade N_2 gas. Quantification of gas products is performed online after an initial electrolysis time of 20 minutes, allowing for cathode

stabilization.

All gas products generated from the cathodic side are connected with a tubing setup to the gas chromatograph (GC, SRI 8610C, SRI) equipped with a molecular sieve of 5A and a Haysep D column. The GC is equipped with a TCD/FID detector with a methanizer, and argon is used as the carrier gas. The partial current density of each gas product is calculated by averaging over 4 GC injections during 1 hour of electrolysis with chronoamperometry.

The liquid product is quantified at the end of each electrolysis using 1H nuclear magnetic resonance (NMR) spectroscopy on a 500 MHz spectrometer (ECA500, JEOL). The initial proton scan is followed by a pre-saturation step to suppress the H_2O peak.

3.3. Chemical state modulation

The chemical state of the tin oxide electrodes on GDL are controlled by post-heat treatment (at 300℃ for 5 hrs in air), and the corresponding oxidation states are determined using X-ray photoelectron spectroscopy (XPS). The O 1s core-level spectra in Figure 3.1A reveals that the surface consists of co-existing SnO and SnO_2 while the post heat treated surface is SnO_2 predominant, which is consistence with our group's previous work. [40] Comparing the valance band maximum (VBM) spectra in Figure 3.1B further supports that SnO is present on the as-prepared surface and it disappears after heat treatment. For further details, please refer to our work [40].

Surface morphology is sustained regardless of heat treatment. The tin oxide electrodes show accumulated spherical particles with gaps between the features (Figure 3.1 C-D). Figure 3.2 reveals no crystalline structure of the tin oxides on GDL is detected from X-ray diffractometry(XRD) regardless of the heat treatment. This is due to the close proximity of the Bragg diffraction angles of graphite with SnO_2 (110), SnO (102), and SnO_2 (220), which results

in a single Bragg diffraction for all samples and thereby difficult for them to be distinguished with confidence. Hereafter, the as-prepared and the post heat treated tin oxides electrodes are denoted as SnO-rich and SnO2-rich catalysts, respectively.

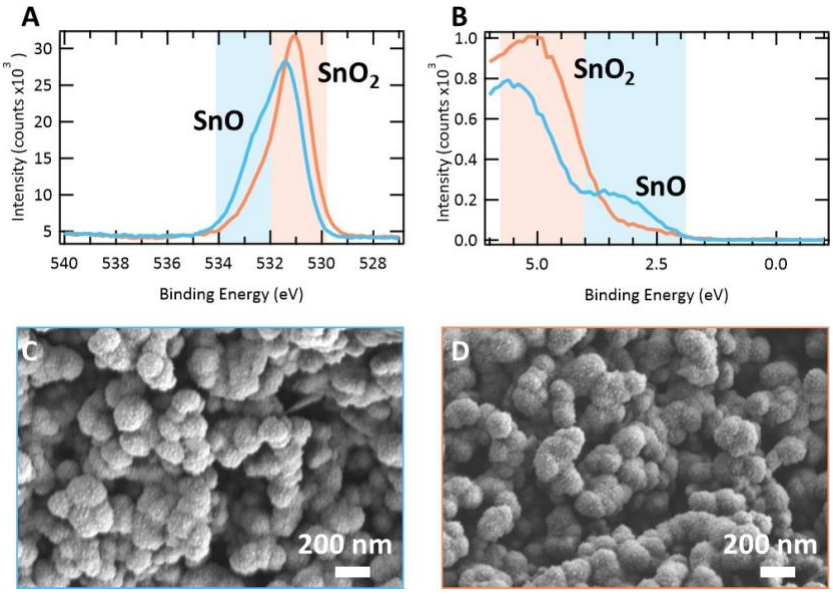

Figure 3.1. Structural properties of tin oxide electrodes. X-ray photoelectron spectroscopy (XPS) of (A) O 1s core level and (B) valence band maximum (VBM) spectra. Scanning electron microscopy (SEM) images of (C) as prepared surface and (D) post heat treated surface.

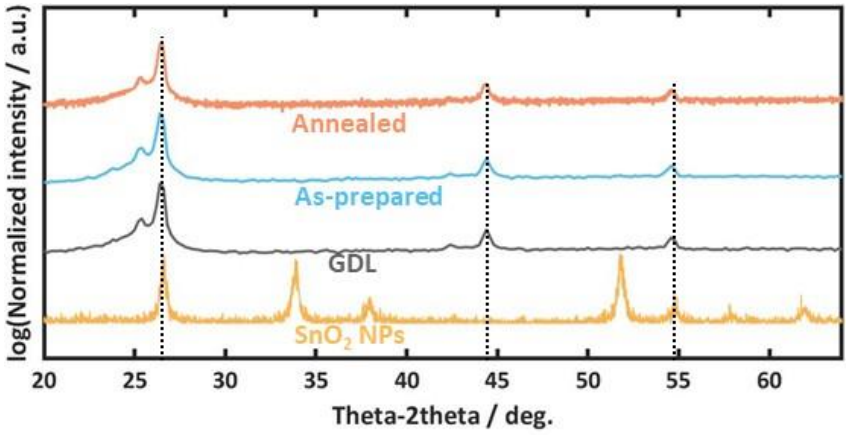

Figure 3.2. The crystalline structure of the Sn oxide electrodes, bare gas diffusion layer, and SnO_2 nanoparticles.

3.4. Effect of Gas Diffusion Layers (GDLs):

The Gas Diffusion Layers, GDLs play an important part as being an intermediate in mass transfer of the CO_2 molecules from the bulk to the catalytic sites. The Gas Diffusion Layers are divided into two categories based on the possession of a micro-porous layer in addition to a macro-porous layer. Here, the Torey 10% PTFE and Torey 30% PTFE do not have a microporous layer whereas Freudenberg H2C36 and AvCarb GDS 2230 have one. Figure 3.3 shows the SEM images for both the GDLs.

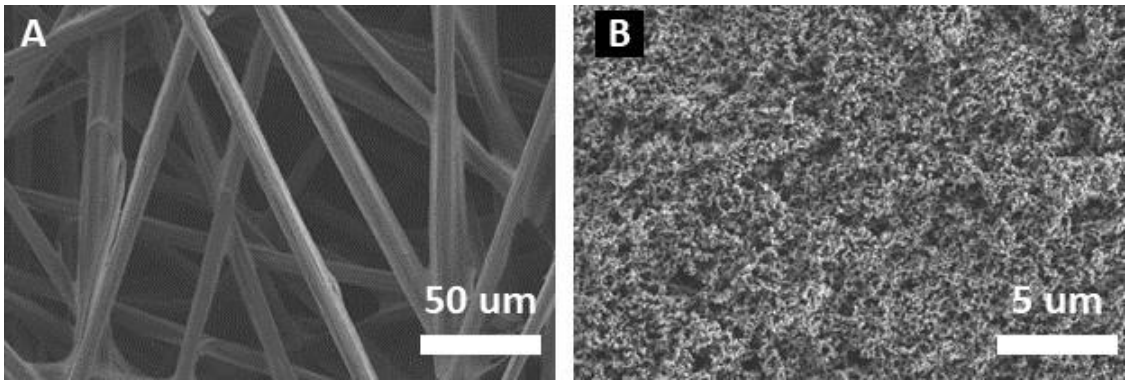

Figure 3.3. Scanning electron microscopy images of GDL surfaces. (A) Macro-porous layer (Toray carbon paper 060 with 10% PTFE content). (B) micro-porous layer (AvCarb GDS2230).

Due to the addition of a micro-porous layer, it aids in the diffusion process of CO_2 and hence CO_2 availability at the catalyst surface is improved [41] In this study, we study the effect of tin oxide evaporated on Toray 060 10% PTFE, Toray 060 30% PTFE, Freudenberg H2C36 and AvCarb GDS 2230 GDLs. We expect the tin oxide coated GDLs with microporous layer to obtain higher activity towards formic acid.

Figure 3.4 shows the faradaic efficiency and partial current density towards formic acid. The formic acid partial current density for SnO_x/AvCarb GDS 2230 (14.812 mA/cm^2_{geo}) is more than 3 times higher that of SnO_x/Toray 30% (4.48 mA/cm^2_{geo}) and Toray 10% (3.14 mA/cm^2_{geo}). This proves our argument of a microporous layer aiding for better diffusion of CO_2 to the catalytic sites and obtaining higher current densities. From here on AvCarb GDS 2230 was used as a GDL for determining effects of other variables.

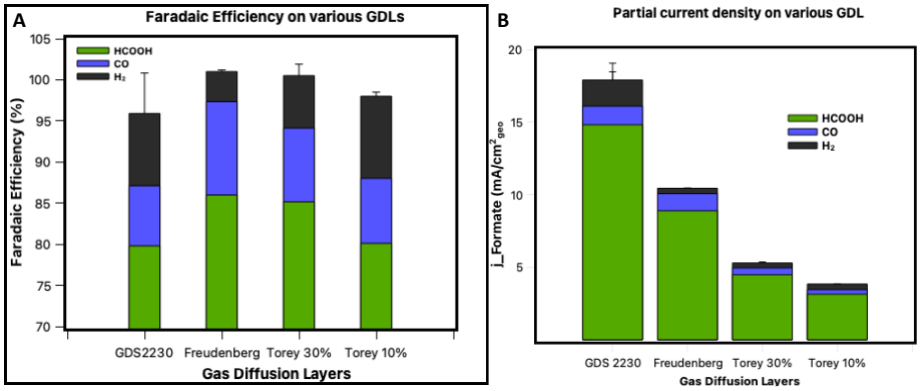

Figure 3.4. Faradaic efficiency (%) [A] and partial current density towards formic acid (mA/cm^2_{geo}) [B] for SnO_x coated on various GDLs.

3.5. Effect of chemical state and applied potential:

In the range of negative cell voltage from -3.0 to -3.4 V, formic acid appears to be the major CO_2 reduction products with marginal formation of CO and hydrogen on the tin oxide catalysts (Figure 3.5). As the applied potential is increased from -3.0 V to -3.4 V, the calculated geometric partial current density of formate on the SnO-rich catalyst increases up to 34.9 mA/cm^2_{geo}, while that of CO is rather consistent fluctuating around 1.6 mA/cm^2_{geo}. The SnO_2-rich catalyst shows similar activities for formic acid and CO, and slightly more activity towards formic acid generation at -3.4 V of cell voltage (46.3 mA/cm^2_{geo}). This indicates that the tin oxide catalysts used here are active for CO_2 electrocatalysis to formic acid.

However, as the cell voltage is increased in the negative direction, hydrogen evolution tends to increase and reaches its maximum at the most negative cell voltage, -3.4 V, on both the catalysts. This means that at high applied potentials, kinetically favored hydrogen evolution starts competing with CO_2 reduction reaction because of the limited mass transport of CO_2 to catalytic sites which in turn results in high partial current density for hydrogen. Overall, shifting oxidation state of the Sn oxide catalysts does not show distinguishable changes in the geometric partial current densities.

In the applied cell potentials, the SnO-rich catalyst shows improved selectivity towards formic acid (80.0 to 82.7 %) as compared to the SnO_2-rich catalyst (~74.0%), as shown in Figure 3.5B. On the contrary, an opposite trend of faradaic efficiency of CO and hydrogen on the cell voltage was observed on both the catalysts, reaching their maximum Faradaic efficiencies are 7.3% and 13.0% at -3.0 and -3.4 V of cell voltage, respectively on SnO rich catalyst.

The SnO-rich catalyst shows stable faradaic efficiency and energy efficiency of formic acid over an extended period of electrolysis at the fixed cell voltage -3.0 V, as shown in Figure 3.5D. The Faradaic efficiency and energy efficiency of formic acid remain essentially unchanged (80.2±0.5% and 36.1±0.2%, respectively) while the Faradaic efficiencies of CO and hydrogen show opposite trends as a function of electrolysis time. The Faradaic efficiency of CO gradually increases from 7.3% to 10.2% while that of hydrogen decreases from 8.8% to 4.2%.

This suggests that CO and hydrogen formation on the tin oxide catalysts are sensitive to the cell voltage while formic acid generation is rather governed by the oxidation state of tin oxides. Corresponding energy efficiency of formic acid in Figure 3.5C shows that SnO-rich catalysts outperform the SnO_2-rich catalyst over the range of cell voltage, with 36.0% of maximum energy efficiency at -3.0 V of cell voltage. With the present grid intensity in California (0.2 $mTCO_2$/MWh) [5,42], this catalytic activity may offer a possible nearest-term path to carbon-negative conversion.

Figure 3.6A shows agglomerated particles on both Sn oxide catalysts after electrolysis, which indicates that the surface morphology evolves during electrolysis. Comparing contact angle of H_2O suggests the agglomerated surface morphology exposes GDL to the surface (Figure 3.6 B-C, which is further confirmed from energy-dispersive X-ray spectroscopy (SEM-EDS), as shown in Figure 3.7. We speculate that these morphological changes and partial exposure of GDL led rise to the parasitic hydrogen evolution thereby impeding the formic acid selectivity slightly.

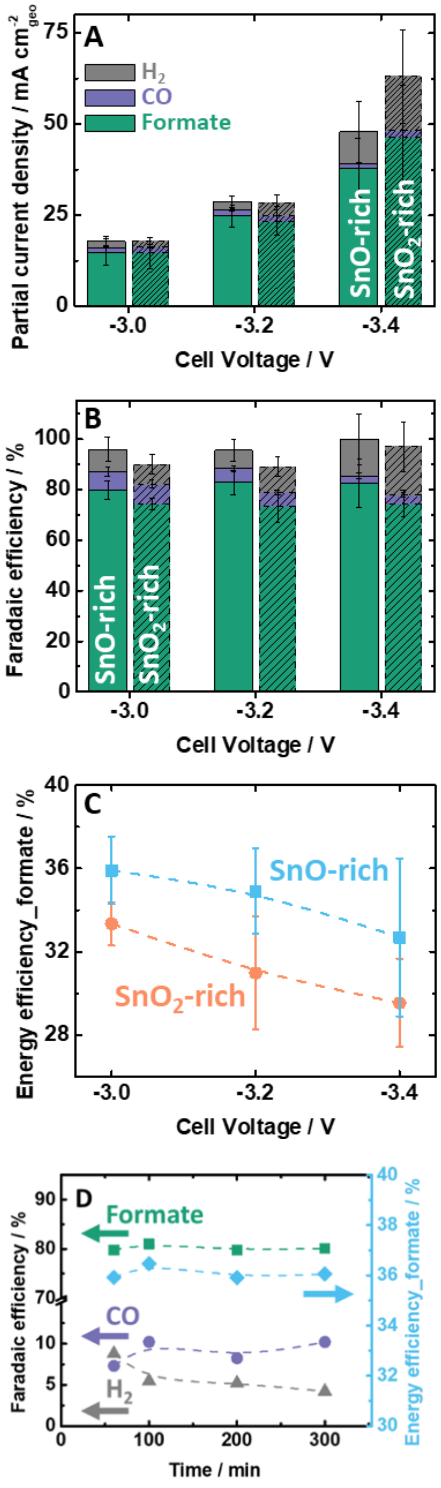

Figure 3.5. CO_2 reduction activities of SnO-rich and SnO_2-rich catalysts as a function of cell voltage. The solid box is for the SnO-rich and the dashed box is for the SnO_2-rich catalyst. (A) geometric partial current densities and (B) Faradaic efficiencies of Hydrogen, CO, and formic acid. (C) Energy efficiency of formic acid on the SnO-/SnO_2-rich catalysts. (D) Long term CO_2 electrocatalysis at -3.0 V applied potential

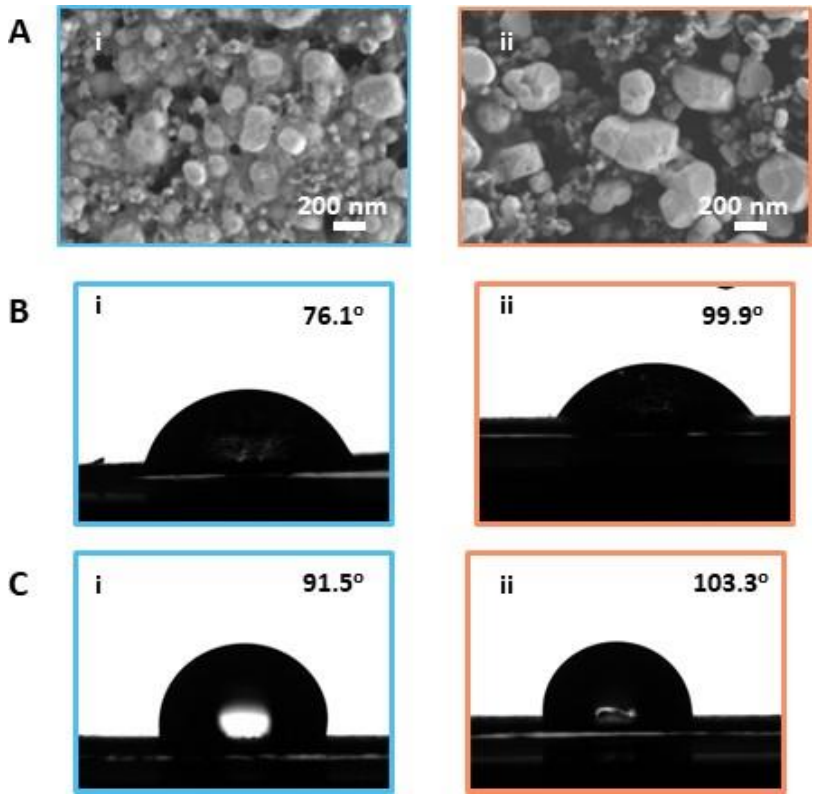

Figure 3.6. Post-electrolysis characterizations. SEM image of A(i) SnO-rich and A(ii) SnO_2- rich catalyst after electrolysis The contact angle of H_2O on SnO-rich B(i) before and C(i)after electrolysis and on SnO_2-rich B(ii) before and C(ii) after electrolysis. The electrolysis is performed for an hour at -3.0 V of cell voltage.

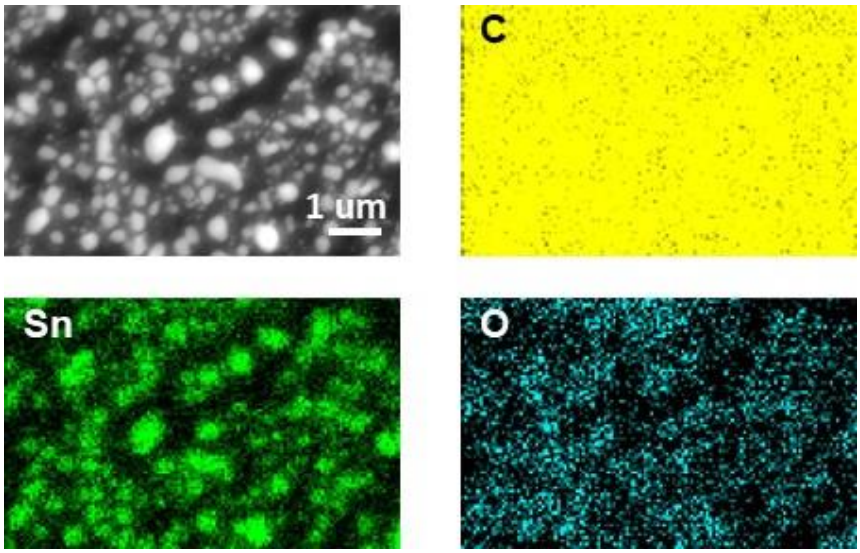

Figure 3.7. SEM-EDS on the SnO-rich catalyst after electrolysis.

3.6 Effect of concentration and flow rate

As the concentration of CO_2 stream is reduced from 100% to 3%, the CO_2 electrocatalytic activity on the catalyst prepared with a SnO-rich surface is reduced due to limited availability CO_2 within the vicinity of the catalyst surface, as shown in the figure 3.8A and C. The geometric partial current density of formic and CO are continuously reduced with decreasing concentration of CO_2 stream while that of hydrogen increases, as shown in the figure 3.8A. It is known that the electrochemical CO_2 conversion to formic acid is a first order reaction as the reaction rate is proportional to the CO_2 concentration [43] which is consistent with our findings in the figure 3.8A.

Figures 3.8 A and B confirm that, regardless of the CO_2 concentration, the CO_2 to formic acid reaction is predominant because of the partial current density of formic acid being 10 times higher than that of CO over the range of CO_2 concentration and that the CO_2 reduction reaction to formic acid is dominantly competing with parasitic hydrogen evolution even at the lowest CO_2 concentration (3%). Meanwhile, the hydrogen evolution reaction increases with decrease in CO_2 concentration due to the limited availability of CO_2 near catalytic sites.

The Faradaic efficiency of formic acid is sustained until 40% CO_2 concentration with only a marginal decrease of 9% and 4% absolute at 100 and 200 ml/min of flow rate, respectively and thereafter it is substantially suppressed at lower CO_2 concentrations, as shown in Figure 3.8B. In addition, in Figure 3.8B and D we observe a tradeoff of selectivity between formic acid and hydrogen, especially below 40% CO_2 concentration, which further emphasizes the importance of CO_2 availability in the electrochemical CO_2 to formic acid conversion.

Increasing flow rate of the pure and partially concentrated CO_2 stream from 100 to 200 ml/min results in ~1.4x higher partial current density of formic acid and ~10% reduction in the partial current densities of CO and hydrogen until 40% CO_2 concentration as shown in Figure 3.8C. Similarly, with an increase in flow rate of CO_2, we observe ~1.3x increase in formate Faradaic efficiency and a 20% decrease in Faradaic efficiency for CO and hydrogen, as shown in Figure 3.8 D. We note that the Faradaic efficiencies of CO and hydrogen at 200 ml/min of CO_2 flow rate in Figure 3.8D are below about 10% each when CO_2 concentration is 40% or above, with substantial suppression of these products relative to the electrolysis at a flow rate of 100 ml/min as shown in figure 3.8B.

However, there exists a tradeoff in selectivity between formic acid and hydrogen below 40% CO_2 concentrations regardless of the CO_2 flow rate which we speculate to be largely attributed to the mass transport of CO_2 to the catalytic sites. Possibly, the increased flow rate of CO_2 helps the diffusion of the generated formic acid away from the catalyst surface to the flow field, which simultaneously facilitates CO_2 transport to the catalytic sites. [44]

To determine rate determining step that governs overall CO_2 reduction activity is by understanding the effect of increasing the CO_2 flow rate. In general, there is a water cross over from the anode to the cathode side due to osmotic drag through membrane in the zero-gap

electrolzyer, and therefore there is a thin layer of water is suggested to be present on the surface of catalyst. [45,46] Adopting a three-phase interface model of gaseous CO_2 - aqueous medium$_{(l)}$ – catalyst$_{(s)}$ in the system, the CO_2 must diffuse through both the GDL and a very thin liquid layer to reach to the catalyst surface as shown in Figure 3.9. At the three-phase interface of CO_2 reduction, the current density is approximately proportional to the CO_2 mass transfer flux, which is a function of mass transfer coefficient and the CO_2 concentration gradient from bulk to the surface [47] as explained by equations 3.1 and 3.2:

$$\Delta C_{CO_2} = [CO_2]_{bulk} - [CO_2]_{surface} \quad (3.1)$$

$$N_{CO_2} = k_c \Delta C = \frac{j}{nF} \quad (3.2)$$

where k_c is the mass transfer coefficient, j is the current density, n is the number of electrons, which is 2 for CO_2 to formic acid conversion, and F is the Faraday's constant.

The high diffusion coefficient of humidified CO_2 in the three-phase interface system (16 mm^2/s) as compared to the two-phase interface system (0.0016 mm^2/s), electrolyte$_{(l)}$ -catalyst$_{(s)}$, typically in the batch cell configuration and also it is assumed that the CO_2 mass transfer flux in the gas phase is identical to that in the liquid because the diffusion length, (x_i) is negligibly thin as compared to the bulk diffusion length, (x_b) as shown in figure 3.9. This means that the CO_2 mass transport through the thin liquid layer may not particularly be the reaction limiting step. Instead, we suggest that the entire CO_2 mass transport from bulk to the catalytic sites is to be rate limiting.

This is consistent with the works of Shi et al., who compared the local CO_2 concentration at the biased catalyst surface between the three-phase (gas-phase CO_2 feed) and the two-phase (solubilized CO_2 feed) interface systems. They emphasize that the CO_2 transportation from the bulk gas phase results in a fast recovery of CO_2 deficiency on the catalytic sites even at high current density (> 50 mA/cm^2) and thereby suggesting that the entire CO_2 mass transport from bulk to the catalytic sites is the reaction limiting step [47].

From theoretical perspective, it is expected that increasing CO_2 flow rate results in increasing mass transfer coefficient (k_c) and consequently enhanced overall CO_2 reduction activity. [48] This further supports that the kinetics of formic acid generation can be improved with facile CO_2 mass transport. Overall, we conclude that the rapid mass transport of CO_2 remains a critical factor of designing CO_2 electrolysis system to enhance CO_2 conversion activity.

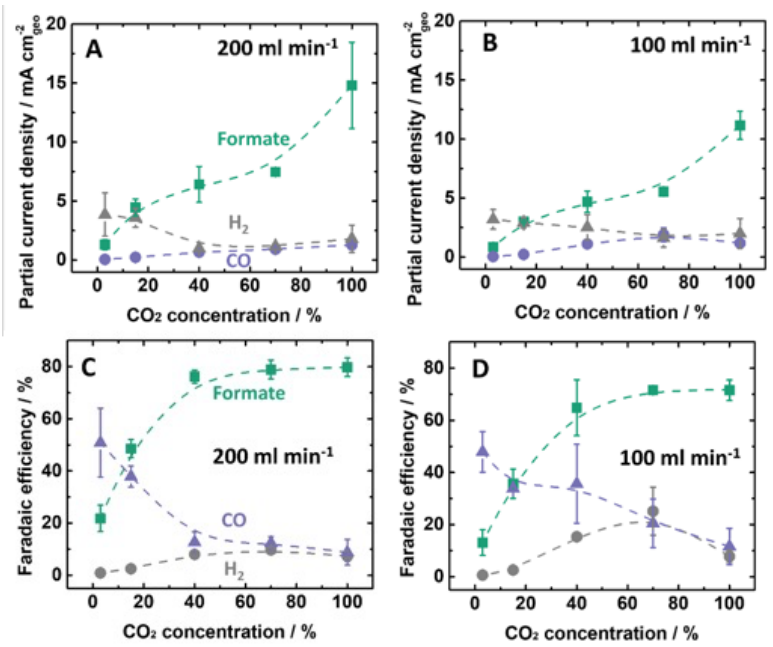

Figure 3.8. Effect of CO_2 flow rate on the catalytic activity with partially concentrated CO_2 stream. The geometric partial current densities and faradaic efficiencies of formic acid (green), CO (purple), and hydrogen (gray) at a flow rate of 100 and 200 ml/min respectively. The CO_2 electrolysis is performed on the SnO-rich catalyst at -3.0 V applied cell voltage for 1 hour with partially concentrated CO_2 stream (3, 15, 40, 70, 100%).

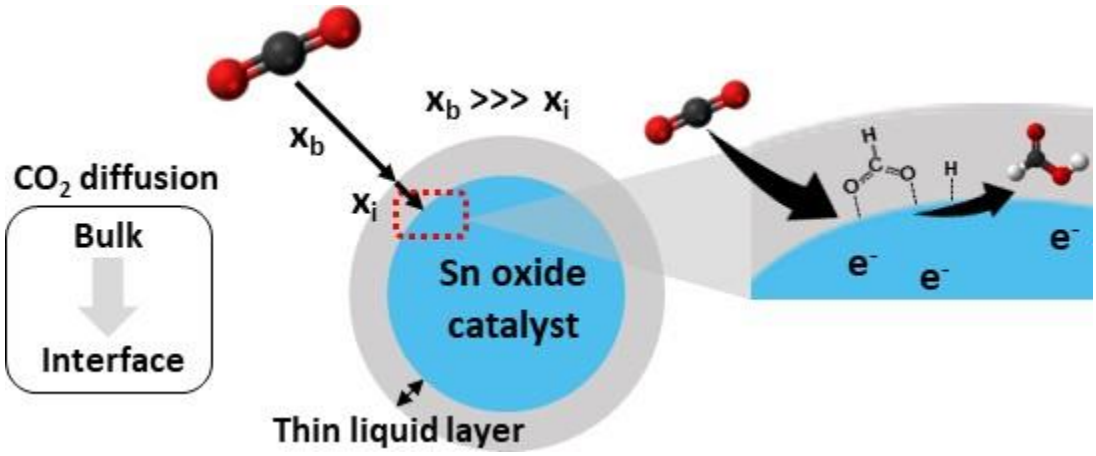

Figure 3.9. Scheme of the simplified CO_2 mass transport to the catalyst surface in a zero-gap MEA electrolyzer. The humidified CO_2 is diffused to the catalyst surface through GDL (bulk) and the thin liquid layer(interface). *OCHO is the reaction intermediate to the formic acid. x_b and x_i are bulk diffusion and internal diffusion path length respectively.

3.7. Summary

In this work, we studied the effect of tuning chemical state of the tin oxides layer for electrochemical conversion of CO_2 to formic acid in a zero-gap MEA electrolyzer. We find a promoted Faradaic efficiency toward formic acid on the tin oxide layer (~83%) where SnO and SnO_2 were co-existed as compared to the SnO_2-rich layer (FE ~74%). The calculated energy efficiency also appears to be improved up to 36% at -3.0 V of applied cell voltage, offering nearest-term net negative CO_2 conversion system. To explore the simulated flue gas composition with partially concentrated CO_2 stream, the energy efficiency and geometric partial current density of formic acid is linearly decreased along with decreasing CO_2 concentration until 40% and subsequently decreasing non-linearly. We find that increasing flow rate of CO_2 facilitates the rapid CO_2 transport onto the catalytic sites and thereby improving the overall kinetics, which confirms that sufficient CO_2 mass transport to the catalytic site is a critical design parameter for CO_2 electrolysis reactor. This work demonstrates that the energy efficiency and activity of electrochemical CO_2 reduction to formic on tin oxide layer can be promoted by modulating the initial oxidation states and flow rate of CO_2 stream even at low CO_2 concentrations. These findings showcase the importance of controlling chemical state of the catalyst and facile mass transport of CO_2 to achieve carbon negative electrochemical CO_2 conversion system.

The observed Faradaic efficiency and geometric partial current density of formate on the SnO-rich catalyst is comparable with the state-of-the-art catalysts as depicted in figure 3.10 [34,49,50].

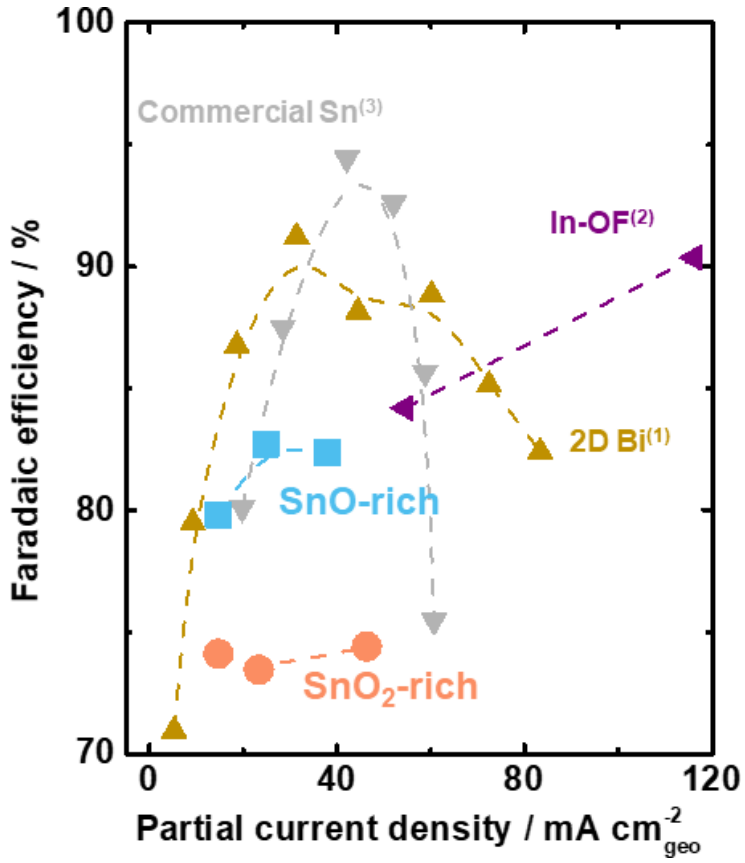

Figure 3.10. Comparison of faradaic efficiency and geometric partial current density on our catalyst with the state-of-the-art catalysts.

3.8. Acknowledgement

Chapter 3, in full, is currently under review for the publication of the material "Tuning oxidation state of SnO_x and Mass Transport to Enhance Catholyte-Free CO_2-to-Formate Electrolysis", Taewoo Kim, **Vivek S. Devalla**, Sean P. Dunfield, Sara Dorr, Moses Kudor, Apoorva Gupta, Jack Palmer and David P. Fenning. The dissertation author was one of the investigators and second author of this material.

Chapter 4

Conclusions and future directions

4.1 Conclusions

Efforts have been made so far to enhance the efficiency of CO_2 conversion systems to achieve carbon neutrality. To improve efficiency, a comprehensive understanding of reaction mechanisms and their correlation with the physicochemical properties of catalytic materials is essential. Additionally, optimizing the design of electrolyzers is crucial for translating insights from the micro-environment to practical operations, ultimately enabling net negative carbon emissions.

This thesis proposes strategies for designing catalytic materials by modulating their chemical environments, which can alter the selectivity and energy efficiency of CO_2 conversion systems. Introducing ligands as a proton source and thereby tuning the environment of catalyst offers a potential means to control the selectivity of CO_2 products. The existence of an optimal pKa ligand on CuS demonstrates improved selectivity in forming formate within an H-Cell system. This study introduces some novel approaches to engineer the catalytic environment of the catalyst and a non-conventional coating technique on to the glassy carbon substrate. However, it also raises some questions regarding the complete exchange of the ligands which in turn is a key parameter for modulating the chemical environment as well as pointing towards the stability and morphology of the catalyst on the glassy carbon surface post reduction reaction. Nevertheless, the results shown in this study is a promising indication of the tuning the micro-environments to steer the chemistry in desired direction.

Additionally, this work proposes strategies for designing catalytic materials by engineering their oxidation states, which can alter the selectivity and energy efficiency of CO_2 conversion systems. Furthermore, it aims to bridge the gap between fundamental understanding and electrolyzer engineering, facilitating further advancements in CO_2 electrolysis. Tuning the chemical state of catalysts offers a potential means to control the selectivity of CO_2 products.

Adjusting the initial surface oxidation state of tin oxide catalysts from SnO_2-rich to a coexistence of SnO and SnO_2 demonstrates improved selectivity and energy efficiency in forming formate within an MEA-type electrolyzer. This research bridges fundamental strategies with pseudo-practical scale investigations. The enhanced energy efficiency achieved with SnO-SnO_2 catalysts in the MEA-type electrolyzer presents a promising approach toward achieving net negative carbon emissions.

Increasing the flow rate of the feed gas to enable rapid mass transport of CO_2 to the catalyst sites can enhance the kinetics of the CO_2-to-formate reaction on tin oxide catalysts, even with partially concentrated CO_2 streams resembling flue gas composition. Experimental confirmation indicates that the rate-limiting step is the mass transport of CO_2, as the electrochemical CO_2-to-formate reaction follows first-order kinetics proportional to the CO_2 concentration, aligning with the findings of this study.

Lastly, it is essential to conduct in-depth studies on electrochemical CO_2 conversion under flue gas conditions where CO_2 concentration is limited, and oxygen is present. Fundamental understandings derived solely from the use of pure CO_2 have limited practicality (e.g., when installing CO_2 conversion systems at the end of point sources like power plants). The presence of oxygen induces other parasitic reactions, such as oxygen reduction, which requires further investigation to increase local CO_2 concentration through ligand engineering, such as incorporating amine functional groups known for their high affinity to CO_2 among different components in flue gas.

4.1 Future Outlook

The future on electrochemical CO_2 reduction holds great promise as a potential solution to mitigate climate change and reduce greenhouse gas emissions. This technology has gained significant attention in recent years due to its ability to simultaneously address two critical challenges: carbon dioxide emissions and the growing demand for sustainable energy storage. One of the key advantages of electrochemical CO_2 reduction is its versatility. By employing different catalysts and tuning reaction conditions, it is possible to selectively produce a wide range of valuable products, including methane, ethylene, formate, ethanol, and more. These products can serve as alternative energy sources or chemical building blocks, displacing fossil fuels and reducing the dependence on non-renewable resources.

Furthermore, the integration of renewable energy sources, such as solar and wind, with electrochemical CO_2 reduction can significantly enhance its sustainability. By utilizing excess renewable electricity during periods of low demand, CO_2 reduction systems can store energy in the form of chemical products, effectively balancing the intermittent nature of renewable energy generation. This approach provides a means to convert and store surplus renewable energy, thereby offering a potential solution to the intermittent power supply challenge.

In conclusion, the outlook on electrochemical CO_2 reduction is highly promising. As research and development efforts continue, we can expect to see significant advancements in catalyst design, system efficiency, and cost reduction, making electrochemical CO_2 reduction a key contributor to sustainable energy and climate change mitigation strategies.

References

[1] United States Environmental Protection Agency.
https://www.epa.gov/ghgemissions/inventory-us-greenhouse-gas-emissions-and-sinks

[2] National Oceanic and Atmospheric Administration.
https://gml.noaa.gov/ccgg/.

[3] United Nations Framework Convention on Climate Change
https://unfccc.int/process-and-meetings/the-paris-agreement

[4] Lazard Levelized Cost of Energy (LCOE) 2020
https://www.lazard.com/media/kwrjairh/lazards-levelized-cost-of-energy-version-140.pdf

[5] Phil De Luna, Christopher Hahn, Drew Higgins, Shaffiq A Jaffer, Thomas F. Jaramillo, and Edward H. Sargent, "What would it take for renewably powered electrosynthesis to displace petrochemical processes?" Science364, eaav3506 (2019)

[6] K. P. Kuhl, T. Hatsukade, E. R. Cave, D. N. Abram, J. Kibsgaard, and T. F. Jaramillo, "Electrocatalytic Conversion of Carbon Dioxide to Methane and Methanol on Transition Metal Surfaces," Journal of the American Chemical Society, vol. 136, no. 40, pp. 14107–14113, 2014.

[7] T. Kim, A. Kargar, Y. Luo, R. Mohammed, E. Martinez-Loran, A. Ganapathi, P. Shah, and D. P. Fenning, "Enhancing C2C3 Production from CO2 on Copper Electrocatalysts via a Potential- Dependent Mesostructure," ACS Applied Energy Materials, vol. 1, no. 5, pp. 1965–1972, 2018.

[8] Kendra P. Kuhl, Etosha R. Cave, David N. Abram, Thomas F. Jaramillo, "New insights into the electrochemical reduction of carbon dioxide on metallic copper surfaces", Energy Environ. Sci., 2012,5, 7050-7059

[9] Ivan Grigioni, Laxmi Kishore Sagar, Yuguang C. Li, Geonhui Lee, Yu Yan, Koen Bertens, Rui Kai Miao, Xue Wang, Jehad Abed, Da Hye Won, F. Pelayo García de Arquer, Alexander H. Ip, David Sinton, and Edward H. Sargent, "CO_2 Electroreduction to Formate at a Partial Current Density of 930 mA cm–2 with InP Colloidal Quantum Dot Derived Catalysts", ACS Energy Lett. 2021, 6, 1, 79–84, 2020

[10] Dou, Tong, Yang Qin, Fazhi Zhang, and Xiaodong Lei, "CuS Nanosheet Arrays for Electrochemical CO2 Reduction with Surface Reconstruction and the Effect on Selective Formation of Formate." ACS Appl. Energy Mater. 2021, 4, 5, 4376–4384

[11] Katherine R. Phillips, Yu Katayama, Jonathan Hwang, and Yang Shao-Horn, “Sulfide-Derived Copper for Electrochemical Conversion of CO_2 to Formic Acid”, J. Phys. Chem. Lett. 2018, 9, 15, 4407–4412

[12] Zhi Cao, Dohyung Kim, Dachao Hong, Yi Yu, Jun Xu, Song Lin, Xiaodong Wen, Eva M. Nichols, Keunhong Jeong, Jeffrey A. Reimer, Peidong Yang, and Christopher J. Chang, “A Molecular Surface Functionalization Approach to Tuning Nanoparticle Electrocatalysts for Carbon Dioxide Reduction”,J. Am. Chem. Soc. 2016, 138, 26, 8120–8125

[13] Yuan Zeng, Paul Hyunggyu Joo, Kesong Yang, and Andrea R. Tao, “Computation-Motivated Design of Ternary Plasmonic Copper Chalcogenide Nanocrystals” , Chem. Mater. 2021, 33, 1, 117–125

[14] Liniker de Sousa, Christian Harmoko, Nieck Benes, and Guido Mul, “Optimizing the Ink Formulation for Preparation of Cu-Based Gas Diffusion Electrodes Yielding Ethylene in Electroreduction of CO_2”, ACS ES&T Engineering 2021 1(12), 1649-1658

[15] Guangxin Liu, David McLaughlin, Simon Thiele, Chuyen Van Pham, “Correlating catalyst ink design and catalyst layer fabrication with electrochemical CO2 reduction performance”, Chemical Engineering Journal, Volume 460, 2023, 141757

[16] Zhuo Xing, Lin Hu, Donald S. Ripatti, Xun Hu, and Xiaofeng Feng, “Enhancing carbon dioxide gas-diffusion electrolysis by creating a hydrophobic catalyst microenvironment”, Nat Commun 12, 136 (2021).

[17] Theresa Jaster, Simon Albers, Armin Leonhard, Mena-Alexander Kräenbring, Heiko Lohmann, Barbara Zeidler-Fandrich, Faith Özcan, Doris Segets, and Ulf-Peter Apfel, “Enhancement of CO_2RR product formation on CuZnO-based electrodes by varying ink formulation and post-treatment methods” 2023 J. Phys. Energy 5 024001

[18] Stefanos Mourdikoudis and Luis M. Liz-Marzán, “Oleylamine in Nanoparticle Synthesis”, Chemistry of Materials 2013 25 (9), 1465-1476

[19] Sohel Das and Subhankar Paul, “Optimized one-pot synthesis of CdSe quantum dot capped with 3-mercaptopropionic acid as an efficient fluorescent probe for selective detection of Hg (II)”, Water and Environmental Journal, Volume 36, Issue 3, 541-552

[20] Xiuhua Zhang and ShengFu Wang, “Voltametric Behavior of Noradrenaline at 2-Mercaptoethanol Self-Assembled Monolayer Modified Gold Electrode and its Analytical Application”, Sensors 2003, 3(3), 61-68

[21] NIST Chemistry WebBook SRD 69, https://webbook.nist.gov/cgi/cbook.cgi?ID=C60242&Mask=80

[22] Lei Fan, Chuan Xia, Peng Zhu, Yingying Lu, and Haotian Wang, "Electrochemical CO_2 reduction to high-concentration pure formic acid solutions in an all-solid-state reactor." Nat Commun 11, 3633 (2020)

[23] Wenchao Ma, Shunji Xie, Xia-Guang Zhang, Fanfei Sun, Jincan Kang, Zheng Jiang, Qinghong Zhang, De-Yin Wu, and Ye Wang, "Promoting electrocatalytic CO2 reduction to formate via sulfur-boosting water activation on indium surfaces", Nat Commun 10, 892 (2019)

[24] Wen Luo, Wei Xie, Mo Li, Jie Zhang, and Andreas Züttel, "3D hierarchical porous indium catalyst for highly efficient electroreduction of CO_2", J. Mater. Chem. A, 2019,7, 4505-4515

[25] Zhu Q, Ma J, Kang X, Sun X, Liu H, Hu J, Liu Z, Han B. "Efficient Reduction of CO2 into Formic Acid on a Lead or Tin Electrode using an Ionic Liquid Catholyte Mixture" Angew Chem Int Ed Engl. 2016

[26] Qing Li, Jiaju Fu, Wenlei Zhu, Zhengzheng Chen, Bo Shen, Liheng Wu, Zheng Xi, Tanyuan Wang, Gang Lu, Jun-jie Zhu, and Shouheng Sun, "Tuning Sn-Catalysis for Electrochemical Reduction of CO2 to CO via the Core/Shell Cu/SnO2 Structure", Journal of the American Chemical Society 2017 139 (12), 4290-4293

[27] Shulin Zhao, Sheng Li, Tao Guo, Shuaishuai Zhang, Jing Wang, Yuping Wu, and Yuhui Chen, "Advances in Sn-Based Catalysts for Electrochemical CO_2 Reduction" Nano-Micro Lett. 11, 62 (2019)

[28] J. T. Feaster, C. Shi, E. R. Cave, T. Hatsukade, D. N. Abram, K. P. Kuhl, C. Hahn, J. K. Nørskov, and T. F. Jaramillo, "Understanding Selectivity for the Electrochemical Reduction of Carbon Dioxide to Formic Acid and Carbon Monoxide on Metal Electrodes," ACS Catalysis, vol. 7, no. 7, pp. 4822–4827, 2017

[29] Y. Chen and M. W. Kanan, "Tin oxide dependence of the CO2 reduction efficiency on tin electrodes and enhanced activity for tin/tin oxide thin-film catalysts," Journal of the American Chemical Society, vol. 134, no. 4, pp. 1986–1989, 2012.

[30] A. Dutta, A. Kuzume, M. Rahaman, S. Vesztergom, and P. Broekmann, "Monitoring the Chemical State of Catalysts for CO2 Electroreduction: An In Operando Study," ACS Catalysis, vol. 5, no. 12, pp. 7498–7502, 2015.

[31] S. Nitopi, E. Bertheussen, S. B. Scott, X. Liu, A. K. Engstfeld, S. Horch, B. Seger, I. E. L. Stephens, K. Chan, C. Hahn, J. K. Nørskov, T. F. Jaramillo, and I. Chorkendorff, "Progress and Perspectives of Electrochemical CO2 Reduction on Copper in Aqueous Electrolyte," Chemical Reviews, vol. 119, no. 12, pp. 7610–7672, 2019.

[32] K. Liu, W. A. Smith, and T. Burdyny, "Introductory Guide to Assembling and Operating Gas Diffusion Electrodes for Electrochemical CO2 Reduction," ACS Energy Letters, vol. 4, no. 3, pp. 639–643, 2019.

[33] D. Higgins, C. Hahn, C. Xiang, T. F. Jaramillo, and A. Z. Weber, "Gas-Diffusion Electrodes for Carbon Dioxide Reduction: A New Paradigm," ACS Energy Letters, vol. 4, no. 1, pp. 317–324, 2019.

[34] W. Lee, Y. E. Kim, M. H. Youn, S. K. Jeong, and K. T. Park, "Catholyte-Free Electrocatalytic CO2 Reduction to Formate," Angewandte Chemie, vol. 130, no. 23, pp. 6999–7003, 2018.

[35] D.Kim,W.Choi,H.W.Lee,S.Y.Lee,Y.Choi,D.K.Lee,W.Kim,J.Na,U.Lee,Y.J. Hwang, and D. H. Won, "Electrocatalytic Reduction of Low Concentrations of CO2 Gas in a Membrane Electrode Assembly Electrolyzer," ACS Energy Letters, vol. 6, no. 10, pp. 3488–3495, 2021.

[36] D. S. Ripatti, T. R. Veltman, and M. W. Kanan, "Carbon Monoxide Gas Diffusion Electrolysis That Produces Concentrated C2 Products with High Single-Pass Conversion," Joule, vol. 3, no. 1, pp. 240–256, 2019.

[37] C. Xia, P. Zhu, Q. Jiang, Y. Pan, W. Liang, E. Stavitsk, H. N. Alshareef, and H. Wang, "Continuous Production of Pure Liquid Fuel Solutions via Electrocatalytic CO2 Reduction Using Solid-Electrolyte Devices," Nature Energy, vol. 4, no. 9, pp. 776–785, 2019.

[38] J. Li, A. Ozden, M. Wan, Y. Hu, F. Li, Y. Wang, R. R. Zamani, D. Ren, Z. Wang, Y. Xu, D. H. Nam, J. Wicks, B. Chen, X. Wang, M. Luo, M. Graetzel, F. Che, E. H. Sargent, and D. Sinton, "Silica-Copper Catalyst Interfaces Enable Carbon-Carbon Coupling towards Ethylene Electrosynthesis," Nature Communications, vol. 12, no. 1, p. 2808, 2021.

[39] T. Kim, G. Kim, D. Lee, Y. Kim, S. E. Shim, and S. Baeck, "Electrochemical Oxidation of Organic Matter in the Prepared via Sol–Gel Methods," Journal of Nanoscience and Nanotechnology, vol. 16, no. 10, pp. 1–6, 2016.

[40] M. Kodur, Z. Dorfman, R. A. Kerner, J. H. Skaggs, T. Kim, S. P. Dunfield, A. Palmstrom, J. J. Berry, and D. P. Fenning, "Electrochemical Screening of Contact Layers for Metal Halide Perovskites," ACS Energy Letters, vol. 7, no. 2, pp. 683–689, 2022

[41] Kailun Yang, Recep Kas, Wilson A. Smith, and Thomas Burdyny, "Role of the Carbon-Based Gas Diffusion Layer on Flooding in a Gas Diffusion Electrode Cell for Electrochemical CO2 Reduction", ACS Energy Letters 2021 6 (1), 33-40

[42] California Independent System Operator (ISO), "Price map," 2022

[43] S. Zhang, P. Kang, and T. J. Meyer, "Nanostructured Tin Catalysts for Selective Electrochemical Reduction of Carbon Dioxide to Formate," Journal of the American Chemical Society, vol. 136, no. 5, pp. 1734–1737, 2014

[44] W. Lee, Y. E. Kim, M. H. Youn, S. K. Jeong and K. T. Park,
Angew. Chemie, 2018, 130, 6999–7003.

[45] W. Lee, Y. E. Kim, M. H. Youn, S. K. Jeong, and K. T. Park, “Catholyte-Free Electrocatalytic CO2 Reduction to Formate,” Angewandte Chemie, vol. 130, no. 23, pp. 6999–7003, 2018.

[46] D. S. Ripatti, T. R. Veltman, and M. W. Kanan, “Carbon Monoxide Gas Diffusion Electrolysis That Produces Concentrated C2 Products with High Single-Pass Conversion,” Joule, vol. 3, no. 1, pp. 240–256, 2019.

[47] R. Shi, J. Guo, X. Zhang, G. I. N. Waterhouse, Z. Han, Y. Zhao, L. Shang, C. Zhou, L. Jiang, and T. Zhang, “Efficient wettability-controlled electroreduction of CO2 to CO at Au/C interfaces,” Nature Communications, vol. 11, no. 1, pp. 1–10, 2020

[48] M. Alfath and C. W. Lee, “Recent Advances in the Catalyst Design and Mass Transport Control for the Electrochemical Reduction of Carbon Dioxide to Formate,” Catalysts, vol. 10, no. 8, p. 589, 2020.

[49] C. Xia, P. Zhu, Q. Jiang, Y. Pan, W. Liang, E. Stavitsk, H. N. Alshareef, and H. Wang, “Continuous Production of Pure Liquid Fuel Solutions via Electrocatalytic CO2 Reduction Using Solid-Electrolyte Devices,” Nature Energy, vol. 4, no. 9, pp. 776–785, 2019

[50] Z. Wang, Y. Zhou, C. Xia, W. Guo, B. You, and B. Y. Xia, “Efficient Electroconversion of Carbon Dioxide to Formate by a Reconstructed Amino-Functionalized Indium–Organic Framework Electrocatalyst,” Angewandte Chemie International Edition, vol. 60, no. 35, pp. 19107–19112, 2021